

# PEGylated and Functionalized Aliphatic Polycarbonate Polyplex Nanoparticles for Intravenous Administration of HDAC5 siRNA in Cancer Therapy

Antoine Frère,<sup>†,§</sup> Alexandra Baroni,<sup>‡</sup> Elodie Hendrick,<sup>§</sup> Anne-Sophie Delvigne,<sup>||</sup> François Orange,<sup>⊥</sup> Olivier Peulen,<sup>#</sup> George R. Dakwar,<sup>∇</sup> Jérôme Diricq,<sup>‡</sup> Philippe Dubois,<sup>‡</sup> Brigitte Evrard,<sup>†</sup> Katrien Remaut,<sup>∇</sup> Kevin Braeckmans,<sup>∇</sup> Stefaan C. De Smedt,<sup>∇</sup> Julie Laloy,<sup>||</sup> Jean-Michel Dogné,<sup>||</sup> Georges Feller,<sup>⊗</sup> Laetitia Mespouille,<sup>‡</sup> Denis Mottet,<sup>§</sup> and Géraldine Piel<sup>\*,†</sup>

<sup>†</sup>Laboratory of Pharmaceutical Technology and Biopharmacy (LTPB) – Center for Interdisciplinary Research on Medicines (CIRM), University of Liege, Avenue Hippocrate 15, 4000 Liege, Belgium

<sup>‡</sup>Laboratory of Polymeric and Composite Materials, Center of Innovation and Research in Materials and Polymers (CIRMAP), Research Institute for Health Sciences and Technology, University of Mons, Place du Parc 20, 7000 Mons, Belgium

<sup>§</sup>Protein Signalisation and Interaction (PSI) – GIGA, University of Liege, Avenue de l'Hopital 11, 4000 Liege, Belgium

<sup>||</sup>Namur Nanosafety Center (NNC), NAMur Research Institute for Life Sciences (NARILIS), Department of Pharmacy, University of Namur, Rue de Bruxelles 61, 5000 Namur, Belgium

<sup>⊥</sup>Centre Commun de Microscopie Appliquée, University of Nice–Sophia Antipolis, Parc Valrose, 06108 Nice, France

<sup>#</sup>Metastasis Research Laboratory (MRL) – GIGA, University of Liege, Avenue Hippocrate 15, 4000 Liege, Belgium

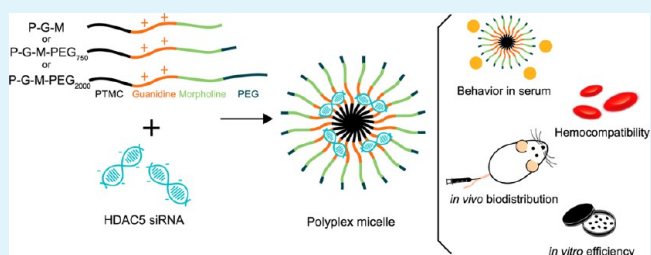
<sup>∇</sup>Laboratory for General Biochemistry and Physical Pharmacy, Ghent Research Group on Nanomedicines, Faculty of Pharmacy, Ghent University, Ottergemsesteenweg 460, 9000 Ghent, Belgium

<sup>⊗</sup>Laboratory of Biochemistry, Centre for Protein Engineering (CIP), University of Liège, Allée du 6 Août 13, 4000 Liège, Belgium

## Supporting Information

**ABSTRACT:** Guanidine and morpholine functionalized aliphatic polycarbonate polymers are able to deliver efficiently histone deacetylase 5 (HDAC5) siRNA into the cytoplasm of cancer cells *in vitro* leading to a decrease of cell proliferation were previously developed. To allow these biodegradable and biocompatible polyplex nanoparticles to overcome the extracellular barriers and be effective *in vivo* after an intravenous injection, polyethylene glycol chains (PEG<sub>750</sub> or PEG<sub>2000</sub>) were grafted on the polymer structure. These nanoparticles showed an average size of about 150 nm and a slightly positive  $\zeta$ -potential with complete siRNA complexation. Behavior of PEGylated and non-PEGylated polyplexes were investigated in the presence of serum, in terms of siRNA complexation (fluorescence correlation spectroscopy), size (dynamic light scattering and single-particle tracking), interaction with proteins (isothermal titration calorimetry) and cellular uptake. Surprisingly, both PEGylated and non-PEGylated formulations presented relatively good behavior in the presence of fetal bovine serum (FBS). Hemocompatibility tests showed no effect of these polyplexes on hemolysis and coagulation. *In vivo* biodistribution in mice was performed and showed a better siRNA accumulation at the tumor site for PEGylated polyplexes. However, cellular uptake in protein-rich conditions showed that PEGylated polyplex lost their ability to interact with biological membranes and enter into cells, showing the importance to perform *in vitro* investigations in physiological conditions closed to *in vivo* situation. *In vitro*, the efficiency of PEGylated nanoparticles decreases compared to non-PEGylated particles, leading to the loss of the antiproliferative effect on cancer cells.

**KEYWORDS:** siRNA, polyplex nanoparticles, intravenous administration, aliphatic polycarbonate, polyethylene glycol, protein corona



## 1. INTRODUCTION

In oncology, histone deacetylases (HDAC) family members are considered as a promising novel class of anticancer targets.<sup>1</sup> These HDAC are actually targeted by broad-spectrum pharmacological HDAC inhibitors (HDACi).<sup>1</sup> These unselective HDACi show promising antitumoral activity both *in vitro*

and *in vivo*. Based on their potent anticancer effects, they are currently being tested in various human clinical trials and some

**Received:** November 23, 2016

**Accepted:** December 28, 2016

**Published:** December 28, 2016

**Table 1.** Characterization of Guanidine and Morpholine Based Aliphatic Polycarbonates Obtained by Organocatalytic ROP of Functional Cyclic Carbonates (DCM, r.t.,  $[M]_0 = 1 \text{ M}$ )

Abbreviation	Sample	DP <sup>a</sup>		$M_n^b$ (g mol <sup>-1</sup> )	$\bar{D}^c$	$N_g^d$ (nmol $\mu\text{g}^{-1}$ )	$N_m^d$	$N_m/N_g$
		CG	CM					
P-G-M	Bz-PTMC <sub>37</sub> -b-PCG <sub>8</sub> -b-PCM <sub>8,5</sub>	8	8.5	10100	1.4	0.79	0.84	1.1
P-G-M-PEG <sub>750</sub>	PEO <sub>750</sub> -PCM <sub>9,5</sub> -b-PCG <sub>8</sub> -b-PTMC <sub>51</sub>	8	9.5	12300	2.2	0.65	0.78	1.2
P-G-M-PEG <sub>2000</sub>	PEO <sub>2000</sub> -PCM <sub>16</sub> -b-PCG <sub>10,5</sub> -b-PTMC <sub>63</sub>	10.5	16	17700	2.2	0.60	0.90	1.5

<sup>a</sup>As obtained by <sup>1</sup>H NMR spectroscopy (500 MHz) in CDCl<sub>3</sub> at r.t. <sup>b</sup>As calculated by <sup>1</sup>H NMR spectroscopy (500 MHz) after BOC deprotection. <sup>c</sup>As obtained by SEC in THF + NEt<sub>3</sub> (2 w%) at 35 °C before BOC deprotection. <sup>d</sup>Concentration of ionizable nitrogen atoms present in the polymer structure (N value), given by guanidinium functions ( $N_g$ ) or morpholine functions ( $N_m$ ) (nmol  $\mu\text{g}^{-1}$ ).

of them like Suberoylanilide hydroxamic acid (SAHA, Vorinostat), Romidepsin (Depsipeptide, FK228, Istodax), Belinostat (PXD101, Beleodaq), and Panobinostat (LBH589, Farydak) were U.S. FDA and/or EMA approved for the treatment of refractory or relapsed cutaneous T-cell lymphomas, validating the concept of HDAC inhibition to treat cancer patients.<sup>2–4</sup> Despite promising results in the treatment of hematological disorders, there is a need to improve the efficacy of these drugs in the clinic.<sup>5</sup> One way for such improvement is the development of more specific inhibitor directed against individual HDAC. By targeting one of the most relevant HDAC members critically involved in tumor progression, it may be possible to greatly improve the efficacy with the additional advantage of removing certain toxicities that may be associated with the inhibition of multiple HDAC.<sup>5</sup> The development of selective pharmacological HDAC inhibitors specifically targeting one HDAC member might be a difficult task, at least because these enzymes share a highly conserved catalytic domain.<sup>6</sup> A siRNA-based strategy might be therefore a better approach to selectively target relevant HDAC for cancer therapy. Preclinical investigations by targeted knockdown of HDAC demonstrated that HDAC5 silencing blocked cell proliferation, cell survival and reduced tumor growth *in vivo* suggesting that selective inhibition of HDAC5 using siRNA could yield clinical benefit for cancer treatment.<sup>7–9</sup>

Since the discovery of RNA interference mechanism (RNAi) at the end of the last century,<sup>10</sup> many researchers have tried to exploit its potential in the treatment of various human diseases, such as cancer.<sup>11,12</sup> The administration of specific small interfering RNA (siRNA) to the cytoplasm leads to the degradation of complementary mRNA (mRNA), and therefore the shutdown of the target protein.<sup>13,14</sup> However, the way into the cytoplasm is paved with extracellular and intracellular barriers. Naked siRNA exhibits a short half-life in the bloodstream due to rapid degradation by serum nucleases.<sup>15</sup> In addition, the high molecular weight and the negative charge also prevent the passage of siRNA through cell membranes. Vectors are thus required to transport and deliver siRNA into the cells. To obtain a therapeutic efficiency, these have to overcome numerous extracellular (nuclease degradation, plasma protein aggregation, recognition by the immune system, tumor accumulation, etc.) as well as intracellular barriers (endocytosis, endosomal escape, and siRNA release into the cytoplasm).<sup>16–20</sup>

To deliver siRNA directed against HDAC5 mRNA, we have previously developed original aliphatic polycarbonate polymers,<sup>21–25</sup> grafted with guanidine and morpholine functional groups. The guanidine function, cationic at neutral pH, is necessary for both siRNA binding and interactions with the negatively charged plasma membranes.<sup>26,27</sup> The morpholine function, weak base and ionizable in acidic pH, confers buffer

capacity to the polymer and helps to escape from the endosome using the “proton sponge” effect.<sup>28</sup> In addition to these functionalized blocks, the polymer contains a hydrophobic chain of poly(trimethylene) carbonate (PTMC), bringing an amphiphilic character to the polymer, and thus allowing it to form nanoparticles in aqueous solution.<sup>29–31</sup> As shown in our previous study,<sup>25</sup> the combination of both morpholine and guanidine functionalities at a ratio above 1 with the presence of a hydrophobic group on the copolymer structure seems to be crucial to overcome intracellular barriers, ultimately leading to protein downregulation activity of siRNA polyplex nanoparticles. This new polycarbonate polymer is called P-G-M for polycarbonate-guanidine-morpholine polymer. Beyond the requested functions to achieve polyplex formation and transport, the aliphatic polycarbonate backbone is fully biocompatible and bioresorbable,<sup>32</sup> making this family of polymer very promising for gene therapy as the vector is degraded after its task is achieved. Such fine-tuned synthetic polymer vector can be produced through a metal-free polymerization process involving nontoxic catalysts in mild conditions and giving access to any kind of functional polymers and topologies.<sup>33–35</sup>

The objective of the present work is to modify further these polymers to enable them to overcome the extracellular barriers and induce biological activity *in vivo* following intravenous injection. Once intravenously injected, polyplexes may interact with different components of the bloodstream. Understanding the influence of the presence of serum on the stability of nanoparticles is crucial to reach a therapeutic efficiency. Indeed, the high amount of anionic serum proteins can interact and cover the surface of cationic nanovectors, forming a “protein corona” around the particle.<sup>36</sup> The formation of this corona changes the identity of the nanovectors. First, the negatively charged proteins can compete with the siRNA on the binding to the nanovectors, resulting in a premature release of the siRNA in the bloodstream.<sup>37</sup> Second, the protein corona can modify the size and the aggregation state, resulting in too large particles for an optimal accumulation at the tumor site through the enhanced permeability and retention (EPR) effect.<sup>38,39</sup> Moreover, aggregation modifies pharmacokinetics which in turn might affect the tissue distribution and penetration.<sup>40</sup> The corona can also change the surface properties of the nanoparticles, lowering the interaction with plasma membranes and thus interfering with cellular uptake and endosomal escape, crucial steps for the polyplex efficiency. In addition, hemocompatibility is a major concern, to safe translation into the clinic, the injection of polyplexes should not cause hemolysis and should not disturb the normal functions of the blood system, like platelet activation and coagulation.<sup>41</sup>

Even if this strategy is sometimes controversial,<sup>42</sup> the most common method to overcome interaction with blood

constituents is PEGylation of nanoparticles. The polyethylene glycol (PEG) shielding around the particle is supposed to reduce the interaction with plasma proteins; depending on the coverage density, the conformation and the molecular weight of PEG chains.<sup>43–45</sup> Two types of PEG were grafted on the previously described polymer: PEG<sub>750</sub> and PEG<sub>2000</sub>. These two polymers (Table 1 and Figure 1) were compared to the non-

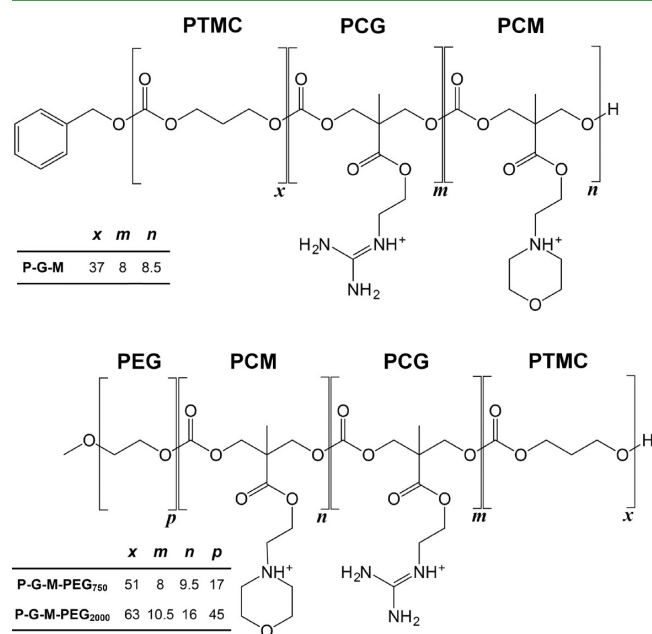


**Figure 1.** Chemical structures of P-G-M, P-G-M-PEG<sub>750</sub>, and P-G-M-PEG<sub>2000</sub> polycarbonate polymers.

PEGylated amphiphatic polycarbonate polymer used in our previous work. The suitability of these nanoparticles for IV injection was evaluated studying siRNA protection against nucleases, behavior in the presence of serum (understanding of nanoparticle–protein interaction, release of siRNA, size stability, and cellular uptake), cytotoxicity and hemocompatibility testing, and *in vivo* tumor accumulation in mouse model. Finally, the biological efficiency of these nanovectors was determined, in order to highlight a decrease of proliferation of cancer cells.

## 2. MATERIALS AND METHODS

**2.1. Materials.** HDAC5 siRNA (sense strand: 5'-CAG-CAU-GAC-CAC-CUG-ACA-ATT-3'; antisense strand: 5'-UUG-UCA-GGU-GGU-CAU-GCU-GTT-3'), GL3 siRNA (sense strand: 5'-CUU-ACG-CUG-AGU-ACU-UCG-ATT-3'; antisense strand: 5'-UCG-AAG-UAC-UCA-GCG-UAA-GTT-3') and Alexa Fluor 546, 647, and 660 labeled siRNAs were provided by Eurogentec (Seraing, Belgium). Nuclease-free water was purchased from Ambion (Life Technologies, Gent, Belgium). 20X TE (Tris-EDTA, pH 7.5) buffer was obtained from Invitrogen (Life Technologies, Gent, Belgium). Mannitol was purchased from Certa (Braine-l'Alleud, Belgium). Heparin sodium salt from porcine intestinal mucosa (200 USP units/mg), and ethidium bromide solution (BET) were provided by Sigma-Aldrich (Diegem, Belgium). Fetal bovine serum (FBS) was obtained from Gibco (Life Technologies, Gent, Belgium).

**2.2. Typical Procedure for the Organocatalytic ROP of Cyclic Carbonates in the Synthesis of Aliphatic Polycarbonate Copolymers.** In a glovebox, a glass vial was charged with the (macro)initiator (BzOH for P-G-M, PEO<sub>750</sub> and PEO<sub>2000</sub> for P-G-M-PEG<sub>750</sub>, and P-G-M-PEG<sub>2000</sub>, respectively), the catalyst (DBU) and methylene chloride. The solution was maintained under magnetic

stirring until homogeneity was reached. Then, the first monomer (TMC for P-G-M, CM for P-G-M-PEG<sub>750</sub>, and P-G-M-PEG<sub>2000</sub>) dissolved in methylene chloride was one-shot added to give a final monomer concentration of 1 M. The initial molar ratio of initiator to catalyst used for each synthesis was 1:5 (ROH:DBU). The vial was sealed and maintained under vigorous stirring until a monomer conversion higher than 90% was reached (as observed by SEC). Polymer chains were directly extended by subsequent addition of the second (Boc-CG) and the third (CM for P-G-M, TMC for P-G-M-PEG<sub>750</sub>, and P-G-M-PEG<sub>2000</sub>) monomers, dissolved in a minimum of DCM, as soon as the previous monomer conversion has reached 90% (as observed by SEC). Polymerizations were quenched with a dash of Amberlyst 15-H and the polymers were recovered after dropwise precipitation in cold *n*-heptane under vigorous stirring. The resulting copolymers were dried overnight under reduced pressure at room temperature. The polymer samples were characterized by SEC in THF + 2 wt % NEt<sub>3</sub> and <sup>1</sup>H NMR in CDCl<sub>3</sub> to determine the macromolecular parameters, as previously described.<sup>25</sup> The Boc protecting groups of the guanidinium moieties were eliminated using TFA in a 5 mL stirred solution of DCM/TFA 4/1 v/v for 18 h at room temperature. Volatiles were removed *in vacuo* and the polymers were dried overnight under reduced pressure at room temperature. Samples were stored into a desiccator maintained under vacuum to avoid moisture entrapment and potential hydrolysis.

**2.3. Polyplexes Formation.** Polyplexes were prepared by electrostatic interaction of the cationic copolymers with the negatively charged siRNA according to the N/P ratio. N/P corresponds to the ratio of the moles of the protonable amino groups (N) on the polymer to the moles of the phosphate groups (P) on siRNA. In practice, the N value corresponds to the concentration of guanidinium + morpholino functionalities (in nmol) per  $\mu$ g of polymer. Polymers were dissolved in TE buffer (pH 7.4, isotonized by mannitol) at a concentration of 1 mg mL<sup>-1</sup>. siRNA was dissolved in the same buffer at a concentration of 1  $\mu$ M. Complexes were obtained by addition of the siRNA solution to the cationic polymer solution, followed by the dilution to the desired concentration of siRNA. The mixture was immediately vortexed for 10 s and left for 30 min at room temperature for polyplexes formation.

**2.4. Size,  $\zeta$ -Potential and siRNA Complexation.** Size and surface charge ( $\zeta$ -potential) of polyplexes were determined at 100 nM of siRNA (N/P 40) using the Zetasizer Nano ZS (Malvern Instruments, UK). The complexation rate of siRNA was determined by the Quant-iT RiboGreen RNA reagent according to the manufacturer's instructions (Invitrogen, Life Technologies, Gent, Belgium).<sup>25</sup>

**2.5. Transmission Electron Microscopy (TEM).** For TEM characterization, nanoparticles were negatively stained using the following procedure: a drop of polyplexes dispersion (5  $\mu$ L, 300 nM siRNA final concentration, N/P 40) was placed on a glow discharged 300 mesh copper grid with a carbon support film for 3 min, and the excess solution was then removed with a filter paper. Staining was performed by adding a drop of 1% uranyl acetate aqueous solution (w/v) on the grid for 2 min and then removing the excess solution. TEM observations were performed with a JEOL JEM-1400 transmission electron microscope, equipped with a Morada camera, at a 100 kV acceleration voltage.

**2.6. Nuclease Resistance.** The protection of siRNA against nucleases when inside polyplexes was evaluated by gel retardation assay. 30  $\mu$ L of polyplexes dispersion (500 nM siRNA, N/P 40) were incubated with or without 1  $\mu$ L of RNase A (50  $\mu$ g/mL, Roche, Basel, Switzerland) for 1 h. Then, 0.5  $\mu$ L of RNaseOUT (Invitrogen, Life Technologies, Gent, Belgium) for RNase A inactivation and 18.5  $\mu$ L of heparin (2 mg/mL, Sigma-Aldrich, Diegem, Belgium) for siRNA release were added. 40  $\mu$ L of these samples mixed with 2  $\mu$ L of glycerol and 2  $\mu$ L of gel blue loading were loaded onto a 4% agarose gel in TAE buffer containing 0.01% ethidium bromide. Electrophoresis was performed at 100 V for 1 h in a Horizon 11.14 horizontal gel electrophoresis apparatus (Biometra, Goettingen, Germany). The gel was visualized by exposure to UV-illumination by a Molecular Imager Gel Doc XR System (Bio-Rad, Hercules, USA). Controls are 300 nM

siRNA, 300 nM siRNA + 1  $\mu$ L of RNase A, and 300 nM siRNA + 0.5  $\mu$ L of RNaseOUT + 1  $\mu$ L of RNase A.

**2.7. Isothermal Titration Calorimetry (ITC).** Interaction of polyplexes with bovine serum albumin (BSA) was evaluated using ITC.<sup>46</sup> ITC titrations were performed on a MicroCal ITC200 (GE-Malvern Instruments, UK) equipped with a 200  $\mu$ L Hastelloy sample cell and an automated 40  $\mu$ L glass syringe rotating at 1000 rpm. To avoid buffer mismatch and the generation of dilution heats, 5 mM BSA (332 mg/mL) (Sigma A7030, fatty acid-, protease-, and globulin-free) were first dialyzed overnight at 4 °C against 200 mM Tris-HCl, 20 mM EDTA, pH 7.5 in RNase free water. Then, the dialysis buffer was used to prepare the nanoparticles. Control experiments indicated negligible heat signals for buffer injections into nanoparticles and dilution heats of BSA injections into buffer were subtracted from experimental data. In a standard experiment, nanoparticles formed by 11.12  $\mu$ M polymer were titrated by 9 injections (4  $\mu$ L) of 5 mM BSA at an interval of 150 s.

The obtained data were fitted via nonlinear least-squares minimization method to determine binding stoichiometry ( $n$ ), association constant ( $K_a$ ), and change in enthalpy of binding ( $\Delta H^\circ_b$ ) using ORIGIN 7 software v.7 (OriginLab). The Gibbs free energy of binding,  $\Delta G^\circ_b$ , was calculated from  $K_a$  and the entropic term,  $T\Delta S^\circ_b$ , was derived from the Gibbs-Helmholtz equation using a fixed  $\Delta H^\circ_b$  value.

**2.8. Fluorescence Correlation Spectroscopy (FCS).** Fluorescence correlation spectroscopy (FCS) was employed to determine the siRNA complexation stability in the presence of fetal bovine serum (FBS). FCS is a microscopy-based technique able to monitor the fluorescence intensity fluctuations of fluorescent siRNA diffusing in and out of the focal volume of a confocal microscope, enabling the determination of the percentage of complexed siRNA.<sup>47</sup> FCS measurements were performed on polyplex nanoparticles containing Alexa Fluor 647 labeled siRNA. 5  $\mu$ L of polyplexes dispersion (300 nM siRNA, N/P 40) was supplemented with TE buffer and FBS to reach a final volume of 50  $\mu$ L, containing 10 or 50% FBS (v/v). Samples were analyzed before FBS addition and after 1, 2, and 3 h incubation at 37 °C following the experimental setup described previously.<sup>37</sup>

**2.9. Fluorescence Single-Particle Tracking (fSPT).** Size stability of polyplexes in the presence of FBS was observed by fluorescence single-particle tracking (fSPT), a microscopy-based technique designed to observe the motion of individual fluorescent nanoparticles in solution. The fluorescent nature of siRNA in polyplex nanoparticles makes them visible in complex media, like FBS. According to the Brownian motion, size distribution can be deduced from the mobility of the sample.<sup>48</sup> fSPT measurements were performed on the same samples used in FCS, after 1 and 3 h of incubation at 37 °C following the experimental setup described previously.<sup>37</sup>

**2.10. Cell Culture (HUVEC, HeLa, and HCT116).** HUVEC primary cells (human umbilical vein endothelial cells) were provided by Lonza (CC-2519, Verviers, Belgium) and cultured in EGM basal medium (Lonza). HeLa cancer cells (human cervical carcinoma cell line) were obtained from Pr. Marc Thiry (GIGA-Neurosciences, University of Liege, Belgium) and cultured at 37 °C in a humidified atmosphere and 5% CO<sub>2</sub> in DMEM (Dulbecco's modified Eagle's medium, Lonza, Verviers, Belgium) supplemented with 10% (v/v) heat inactivated fetal bovine serum (FBS, Gibco, Life Technologies, Gent, Belgium). HCT116 cancer cells (human colorectal carcinoma cell line) were provided by Pr. Eric Verdin (Gladstone Institute, University of California, USA) and cultured in McCoy's 5A (Lonza) supplemented with 10% heat inactivated FBS.

**2.11. Cell Viability (MTS) and Cytotoxicity (LDH) Assays.** HUVEC were seeded in a 96-well plate at a density of  $8 \times 10^4$  cells/well and incubated for 48 h. Polyplex nanoparticles, at a concentration of 100 nM GL3 siRNA (N/P 40), were added to the cells in 100  $\mu$ L of Opti-MEM and incubated for 3 h and then washed. Cell viability and cytotoxicity of polyplex nanoparticles were determined 24 h later using MTS assay (CellTiter 96 AQueous One Solution Cell Proliferation Assay, Promega, WI, USA) or LDH assay (Cytotoxicity Detection Kit<sup>PLUS</sup>, Roche, Basel, Switzerland), according to manufacturers' instructions.

**2.12. Hemocompatibility Assays.** Hemolysis, platelet aggregation, and coagulation (calibrated thrombin generation test) were tested using protocols described previously<sup>31</sup> and using a final concentration of polyplex nanoparticles of 100 nM GL3 siRNA (N/P 40). For hemolysis assay, Triton X-100 (1%) was used as technical positive control to fix the 100% hemolysis value.

**2.13. In Vivo Biodistribution in Mice.** All procedures for xenograft tumor mouse model were approved by the Animal Welfare Committee of the University of Liege (approval #1748).  $3 \times 10^6$  HeLa cells in 200  $\mu$ L PBS were subcutaneously injected into the right flank of 8 weeks-old male NOD-SCID mice (Charles River, MA, USA). Four weeks after inoculation, when the tumor size reached  $\sim 500$  mm<sup>3</sup>, a single dose of polyplexes containing 1 mg/kg Alexa Fluor 660 HDAC5 siRNA at N/P 40 (100  $\mu$ L) was injected into the tail vein. Four hours postinjection, mice were anesthetized with isoflurane and images of the full animal fluorescence were recorded by Xenogen IVIS-200 System (PerkinElmer, MA, USA) using Cy5.5 filters. Mice were then sacrificed and fluorescence intensity of their organs was examined *ex vivo*.

**2.14. Cellular Uptake.** Alexa Fluor 546 labeled siRNA fluorescent polyplexes were formed at a concentration of 600 nM (N/P 40) and then diluted to 100 nM in Opti-MEM (Invitrogen, Gent, Belgium) and FBS to reach a final concentration of 0, 10, 30, or 50% FBS (v/v). These samples were preincubated 1 h at 37 °C and then added to HeLa cells for 3 h. Cells were washed with PBS, trypsinized and collected into complete DMEM medium. Samples were centrifuged 4 min at 250 g at room temperature and suspended in 350  $\mu$ L PBS.  $10^4$  cells were analyzed using a FACSCalibur flow cytometer (BD Biosciences, FACSCalibur, USA). Data were analyzed using CellQuest Pro software (BD Biosciences, USA).

**2.15. RT-qPCR.** mRNA expression was determined on HeLa cells 48 h after transfection, using quantitative real-time PCR. Protocol is detailed in our previous publication.<sup>25</sup> In the case of a second treatment, transfection was repeated after 24 h and cells were incubated for the remaining 24 h.

**2.16. Proliferation Assay and Western Blot.**  $4 \times 10^4$  transfected HCT116 cells were seeded in 24-well tissue culture plates in complete medium and were harvested at the indicated time-points. The cell numbers were indirectly determined using Hoechst incorporation (Bisbenzimidazole H33258, Calbiochem, Merck, Nottingham, UK), as previously described.<sup>49</sup> Protein expression in these cells at different time points was determined by Western blot using the protocol described in our previous work.<sup>25</sup>

**2.17. Statistical Analysis.** Experiments were performed in triplicate ( $n = 3$ ), unless otherwise stated. Values are given as means  $\pm$  standard deviation (SD). Statistical tests used are described in legends of related figures. \*  $p < 0.05$ , \*\*  $p < 0.01$ , or \*\*\*  $p < 0.001$  were considered statistically significant.

### 3. RESULTS

**3.1. Polyplexes Characterization and siRNA Complexation.** Formation of polyplexes is due to electrostatic interaction between cationic functional groups present on the polymer structure with anionic phosphate function of the siRNA. Size,  $\zeta$ -potential and complexation of siRNA are closely related to the N/P ratio. To select the optimal N/P ratio, particles were characterized in buffer from N/P 10 to N/P 60, at a fixed siRNA concentration of 100 nM (Figure S1). Based on these results, an optimal N/P ratio of 40 was selected for next experiments. N/P 40 is the minimum ratio to achieve a maximal encapsulation of the siRNA (close to 100%) while reaching the surface size and charge equilibrium and avoiding an excess of polymer.

Physicochemical characteristics at N/P 40 are detailed in Table 2. PEGylated and non-PEGylated polyplexes show similar siRNA complexation capacities, around 100%. The hydrodynamic diameter was slightly higher for the non-

**Table 2.** Physicochemical Characteristics of Polyplex Nanoparticles at N/P 40<sup>a</sup>

Polyplex nanoparticle	Size (nm)	PDI	$\zeta$ -potential (mV)	siRNA complexation (%)
P-G-M	223 ± 18	0.24 ± 0.05	11.2 ± 0.9	100.4 ± 0.4
P-G-M-PEG <sub>750</sub>	151 ± 20	0.22 ± 0.02	8.2 ± 1.1	97.8 ± 0.6
P-G-M-PEG <sub>2000</sub>	150 ± 25	0.34 ± 0.08	5.0 ± 0.9	100.0 ± 0.1

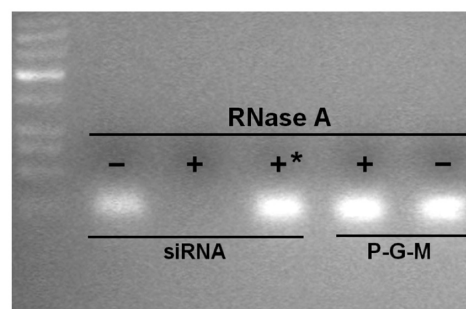
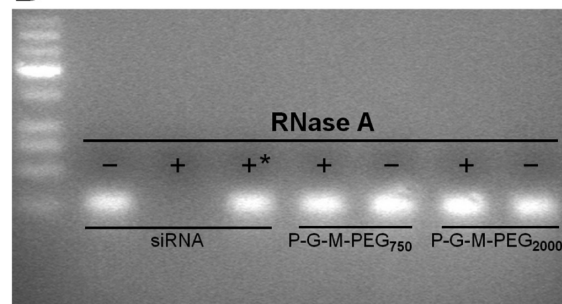
<sup>a</sup>Values represent mean ± SD (*n* = 3).

PEGylated polymer (P-G-M). The polydispersity index (PDI) was below 0.3 for P-G-M and P-G-M-PEG<sub>750</sub>, indicating nearly monodisperse sample. P-G-M-PEG<sub>2000</sub>, with a PDI of 0.34, presents a higher but moderate polydispersity.

Morphology of these nanoparticles was determined by transmission electron microscopy (TEM). TEM images at different magnifications (Figure 2) show the spherical morphology of polyplex nanoparticles. The three samples show a smaller size with TEM, around 100 nm, than values measured by DLS (Table 2). This is due to the fact that DLS determines the hydrodynamic diameter of samples in the aqueous buffer, whereas TEM measures size of particles in the dry state.

**3.2. Nuclease Resistance.** To verify the ability of polymers to protect siRNA from nucleases, gel retardation assay was performed after incubation with RNase A for 1 h, followed by its inhibition by RNase OUT, and the release of siRNA from polyplexes with heparin. Figure 3 shows that the siRNA is protected when complexed in both PEGylated (Figure 3B) and non-PEGylated (Figure 3A) polyplex nanoparticles compared to naked control siRNA, which is immediately fully degraded.

**3.3. Polyplexes Behavior in the Presence of FBS.** Behavior of PEGylated and non-PEGylated nanoparticles in the

**A****B**

\*RNase OUT added before RNase A

**Figure 3.** Nuclease resistance of siRNA complexed in polyplex nanoparticles. Gel retardation assay was performed after incubation in presence (+) or absence of (–) RNase A for 1 h, followed by its inhibition by RNase OUT, and the release of siRNA with heparin. (A, P-G-M; B, P-G-M-PEG<sub>750</sub> and P-G-M-PEG<sub>2000</sub>).

presence of serum was evaluated using different techniques. First, interaction of polyplex nanoparticles with BSA was evaluated using ITC. Then, the effect of PEG<sub>750</sub> and PEG<sub>2000</sub> grafted polymers on behavior in the presence of FBS was

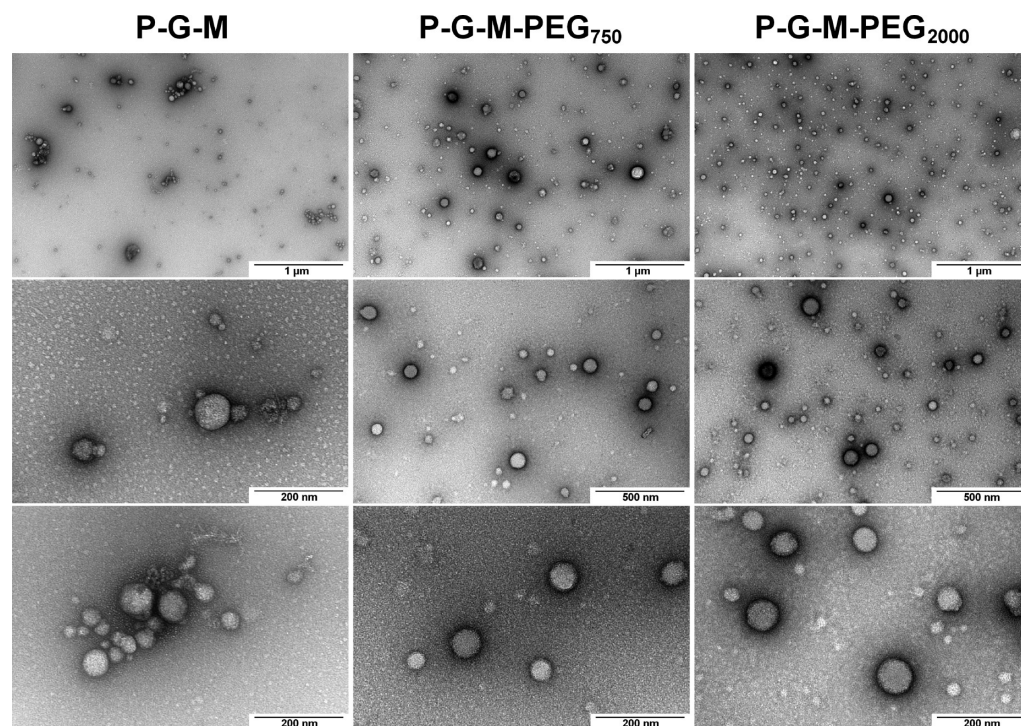


**Figure 2.** TEM images of P-G-M, P-G-M-PEG<sub>750</sub>, and P-G-M-PEG<sub>2000</sub> polyplexes at different magnifications.

evaluated in terms of siRNA release (FCS) and aggregation (fSPT), compared to non-PEGylated polyplexes.

**3.3.1. Interaction of Polyplexes with BSA.** To study the interactions of the investigated nanoparticles with serum proteins, nanoparticles were titrated with BSA, a blood model protein, using ITC. This system records the heat generated by the association of the binder with its ligand and following progressive saturation, the binding enthalpy, the affinity constant and the stoichiometry are usually derived by fitting of a Wiseman plot (Figure 4). Titration of the investigated

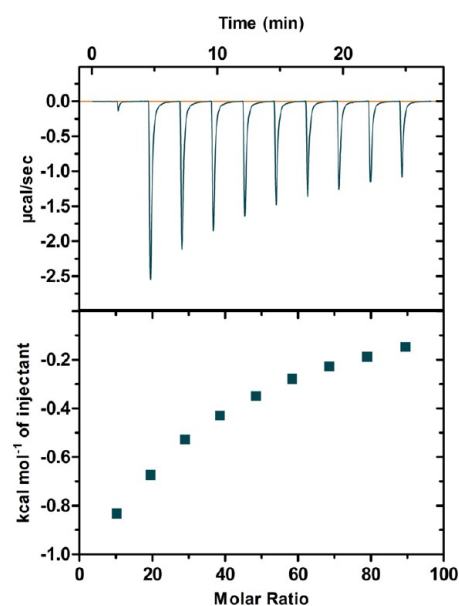


**Figure 4.** Isothermal titration calorimetry of BSA binding to polyplex nanoparticles P-G-M-PEG<sub>2000</sub> at 25 °C. Upper panel: exothermic microcalorimetric traces of BSA (5 mM) injections into nanoparticle solution (11 μM). Lower panel: Wiseman plot of heat releases versus molar ratio of injectant/polymer in the cell.

nanoparticles with BSA showed a low affinity system, with dissociation constants in the mM range. For such low affinity systems, full saturation by the ligand cannot be reached even at the high concentration of BSA used which is the maximal solubility limit in the titration syringe. Accordingly, only a partial binding isotherm is recorded (Figure 4) and one of the fitted variables has to be kept constant.<sup>50</sup> In previous studies, stoichiometry was the fixed variable as this parameter can be confidently obtained from known chemical or macromolecular structures. This is obviously not valid for nanoparticles that can bind an unknown number of protein molecules. However, the binding enthalpies are generally in the range of 5 kcal/mol and this value was kept constant for a comparative analysis. Accordingly, the reported data should be regarded as apparent values. As indicated in Table 3, the BSA binding ability of the three types of nanoparticles does not differ significantly, although P-G-M-PEG<sub>2000</sub> displays a slightly lower affinity

constant  $K_a$  for the serum protein. All particles roughly bind a 10-fold molar excess of BSA ( $n$ ) with respect to polymer concentration. The enthalpic and entropic contributions to  $\Delta G^\circ_b$  suggest that the association is enthalpy-driven (favorable interactions such as H-bonds or van de Waals contacts) whereas the weak and unfavorable entropy may reflect a reduction of the degree of freedom upon BSA binding. This weak and unfavorable entropic term also suggests that the hydrophobic effect is not significantly involved in BSA binding.<sup>51</sup>

**3.3.2. siRNA Release in the Presence of FBS.** The possible destabilization of polyplexes by serum proteins and so, the siRNA release was determined using FCS before and after 1, 2, and 3 h of incubation with 10% or 50% FBS (v/v). Figure 5 shows the percentage of complexed siRNA over time, in 10% (A) or 50% FBS (B). In the presence of 10% FBS, the release of siRNA is low, especially for non-PEGylated polyplexes (P-G-M). After 3 h, 13%, 31%, and 35% of siRNA are released from P-G-M, P-G-M-PEG<sub>750</sub>, and P-G-M-PEG<sub>2000</sub>, respectively. In the presence of 50% FBS, around 50% siRNA is released from both PEGylated and non-PEGylated formulations after 1 h. However, this siRNA release remains constant up to 3 h of incubation.

**3.3.3. Size Distribution in the Presence of FBS.** The size distribution and aggregation profile of the studied formulations was obtained by fSPT, a powerful technique to follow the size of fluorescent nanoparticles in a protein-rich medium, like FBS. The great advantage of this method compared to DLS is the possibility to detect only fluorescent nanoparticles, not taking into account all other components of biological fluids (e.g., proteins, enzymes, etc.), whereas DLS is best suited for aqueous solutions. Size distributions in TE buffer, and after 1 or 3 h incubation with 10% FBS were compared. In TE buffer, the average diameter of P-G-M polyplexes (Figure 5C) was around 220 nm. One hour after FBS incubation, the size distribution became bimodal, with a peak around 111 nm and the second peak around 450 nm. After 3 h, the intensity of the 450 nm peak increased while the 111 nm peak decrease, showing an increase in size of the polyplexes over time. For P-G-M-PEG<sub>750</sub> particles (Figure 5D), the average size in buffer was 135 nm, increasing to 275 nm after 1 h of incubation with FBS. Between 1 and 3 h, the size remains constant, but with an initial increase of size in the presence of FBS. Finally, P-G-M-PEG<sub>2000</sub> polyplexes (Figure 5E) showed a size around 260 nm in buffer. However, the behavior in the presence of FBS is similar to P-G-M-PEG<sub>750</sub> polyplexes, with an initial increase of the size becoming stable after 1 h (around 510 nm). These size distributions were also evaluated by DLS (Figure S3–S4). DLS results show that the size increase is greater for non-PEGylated compared to PEGylated polyplexes, with a diameter around 600–700 nm. The size of P-G-M-PEG<sub>750</sub> and P-G-M-PEG<sub>2000</sub> is around 300 nm directly after FBS addition, increasing slightly and stabilizing close to 400 nm, from 1 to 3 h. Unfortunately, it was not possible to record size distribution in 50% FBS due to

**Table 3. Binding Parameters of BSA Association with Nanoparticles at 25 °C**

Polyplex nanoparticle	$n$	$K_a$ ( $10^3$ M <sup>-1</sup> )	$\Delta G^\circ_b$ (kcal mol <sup>-1</sup> )	$\Delta H^\circ_b$ <sup>a</sup> (kcal mol <sup>-1</sup> )	$T\Delta S^\circ_b$ (kcal mol <sup>-1</sup> )
P-G-M	9.7 ± 0.3	2.1 ± 0.1	-4.5	-5.0	-0.5
P-G-M-PEG <sub>750</sub>	9.1 ± 0.2	2.3 ± 0.1	-4.6	-5.0	-0.4
P-G-M-PEG <sub>2000</sub>	12.8 ± 0.2	1.7 ± 0.1	-4.4	-5.0	-0.6

<sup>a</sup>Fixed value for nonlinear fit of the binding isotherm for  $n$  equivalent binding sites.

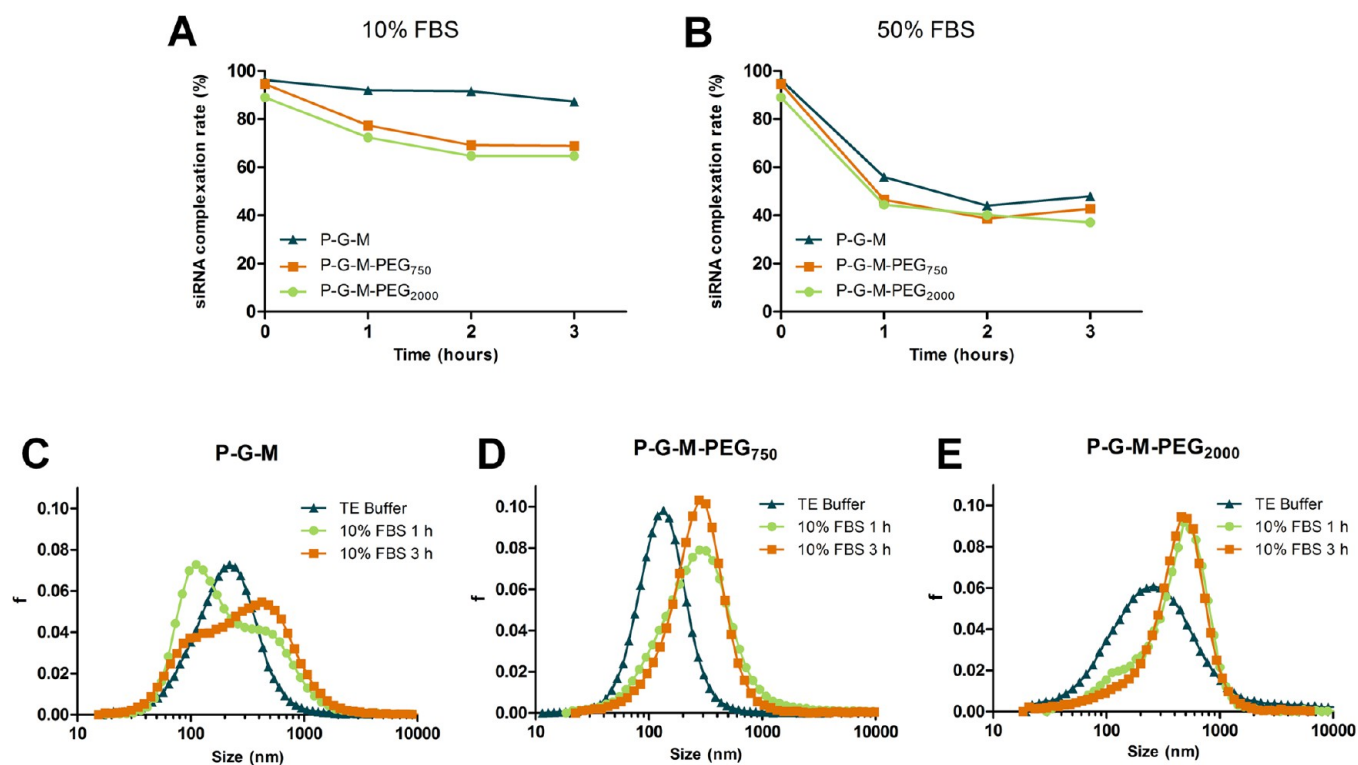


**Figure 5.** siRNA complexation rate and size evolution in the presence of FBS. siRNA complexation rate of the three different polyplexes determined by FCS, in TE buffer (time = 0) and following 1, 2, and 3 h incubation at 37 °C with 10% (A) or 50% FBS (B). Size distributions determined by fSPT, in TE buffer and following 1 and 3 h incubation in 10% FBS at 37 °C, for P-G-M (C), P-G-M-PEG<sub>750</sub> (D), and P-G-M-PEG<sub>2000</sub> polyplexes (E). The Y-axis refers to the fraction (*f*) of polyplexes that appear with the corresponding size on the X-axis.

the 50% release of siRNA, making the dispersion medium too fluorescent to clearly distinguish diffusing nanoparticles.

**3.4. Toxicity on Endothelial Cells (HUVEC).** *In vivo*, before to reach the cells, polyplex particles will be in contact with various elements dispersed in blood that can interact with the particles together with negatively charged blood vessel endothelium. Endothelial cells are one of the first elements that polyplex nanoparticles will encounter. To have an idea of the toxicity of polyplexes for blood vessel endothelium, the toxicity on primary human endothelial cells (HUVEC) was evaluated *in vitro* using MTS viability and LDH cytotoxicity assays. Cells were treated for 3 h with 100 nM siRNA complexed with the three different polymers and cytotoxicity was measured 24 h later. As shown in Figure 6, both MTS and LDH assay demonstrate that the cytotoxicity of these polycarbonate polymers is low and nonsignificantly different from the negative control (PBS).

**3.5. Hemocompatibility.** To evaluate the compatibility of polyplex nanoparticles formulation with an intravenous injection, hemocompatibility assays were performed. Results show that P-G-M, P-G-M-PEG<sub>750</sub>, and P-G-M-PEG<sub>2000</sub> nanoparticles did not induce hemolysis in whole blood (Figure 7A) and in washed RBC (Figure S5A). Next, platelet aggregation was evaluated, after 1 h of incubation, in the presence of different polyplex nanoparticles and different inducers (Figure 7B for collagen, Figure S5B for ADP and S5C for arachidonic acid). At the investigated concentrations, P-G-M, P-G-M-PEG<sub>750</sub>, and P-G-M-PEG<sub>2000</sub> did not significantly affect platelet aggregation, regardless the inducer used. Finally, to evaluate their potential interferences on coagulation process, nanoparticle formulations were tested with calibrated thrombin generation test. Figure 7C shows representative thrombin

activity profile induced by tissue factor in the presence of polyplex nanoparticles. From these profiles, control parameters (lag time (Figure 7D), peak (Figure 7E), and endogenous thrombin potential (ETP) (Figure 7F)) were extracted, normalized and compared to negative control, PBS. No significant difference was observed, showing no pro- or anticoagulation activity.

**3.6. *In Vivo* Biodistribution on Mice.** The *in vivo* biodistribution of Alexa Fluor 660 HDAC5 labeled siRNA delivered alone or complexed with P-G-M, P-G-M-PEG<sub>750</sub>, or P-G-M-PEG<sub>2000</sub> polyplex nanoparticles was examined after intravenous (IV) administration. First, we followed the accumulation of polyplexes in living mice 4 and 24 h post injection of 1 mg/kg fluorescent siRNA in P-G-M-PEG<sub>750</sub>. Figure 8A shows that the siRNA already accumulates at the tumor site 4 h post IV injection. This fluorescence at the tumor site decreases but still remains after 24 h. Experiments of *ex vivo* imaging on tumors and principal organs were therefore performed 4 h post IV injection. Figure 8B shows a tumor accumulation of Alexa Fluor 660 siRNA only in mice treated with P-G-M, P-G-M-PEG<sub>750</sub>, and P-G-M-PEG<sub>2000</sub> polyplex nanoparticles. No siRNA was detected in the tumors when mice were untreated or treated with free siRNA. Fluorescent siRNA was detected in the liver in all conditions except untreated mice, as well as in kidneys and the spleen, but in a lower level. P-G-M polyplexes show a high accumulation in lungs. 24 h postinjection, mouse was sacrificed. Among the different dissected organs, a slight fluorescent signal in liver tissue has been observed (data not shown). To distinguish better the difference between tumors, fluorescence of the same tumors but with a different fluorescence scale is shown on

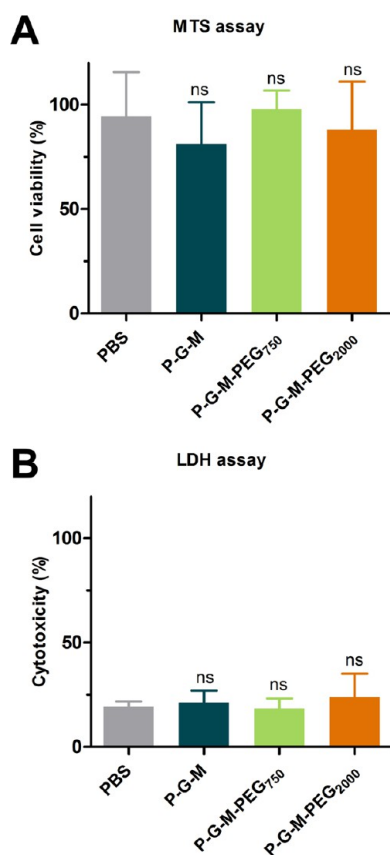


**Figure 6.** Toxicity of polyplex nanoparticles on primary endothelial cells. (A) Cell viability (MTS assay) of HUVEC cells treated for 3 h with different nanoparticles at a concentration of 100 nM in siRNA, washed and then cultured for additional 24 h. The percentage is related to nontreated cells (100%), and blank wells without cells (0%). (B) Cytotoxicity (LDH assay) of HUVEC cells treated for 3 h with different nanoparticles at a concentration of 100 nM in siRNA, washed and then cultured for additional 24 h. The percentage is related to positive control (Triton X-100 1%, cytotoxicity of 100%), and blank wells (without cells, cytotoxicity of 0%). Statistical comparison with negative control (PBS) was performed by using one-way ANOVA, followed by the Dunnett's test ( $n = 4$ ).

**Figure 8C.** Fluorescence seems to be slightly lower in tumors treated with P-G-M.

**3.7. Cellular Uptake.** Cellular uptake was first determined in serum-free conditions (Opti-MEM). To evaluate the effect of high amount of proteins in the medium on the cellular uptake, flow cytometry was performed after preincubation of polyplexes in medium supplemented with 10, 30, or 50% FBS. The mean fluorescent intensity (MFI) of HeLa cells was evaluated 3 h after transfection, indicating the mean amount of fluorescent siRNA uptaken by cells.

In serum-free conditions (Figure 9), P-G-M and P-G-M-PEG<sub>750</sub> nanoparticles present a significantly better uptake than P-G-M-PEG<sub>2000</sub>. After 1 h of preincubation in 10% FBS, the cellular uptake is significantly decreased, except for P-G-M-PEG<sub>2000</sub>. The cellular uptake of these nanoparticles is not significantly different from serum-free conditions, contrarily to P-G-M and P-G-M-PEG<sub>750</sub>. With 30% and 50% FBS, the decreased uptake is even more pronounced for the PEGylated nanoparticles, with a MFI close to 0 compared to non-PEGylated polyplexes.

### 3.8. In Vitro Efficiency: mRNA, Protein Silencing, and Biological Activity.

The ability of polyplexes to decrease the expression of HDAC5 mRNA was investigated by quantitative real-time RT-PCR, 48 h after the treatment of HeLa cells in serum-free conditions. To exclude nonspecific effects of polymers, the relative HDAC5 mRNA expression was normalized to cells treated with the same polyplexes but containing irrelevant GL3 siRNA. The mRNA shutdown was evaluated after 1 and 2 treatments with polyplexes. As shown in our previous publication, the P-G-M polyplexes were capable of decreasing the expression of HDAC5 (mRNA and protein) of about 50% after one treatment.<sup>25</sup> With a second transfection, efficiency was increased: the relative mRNA expression was reduced from 50% to 20% (Figure 10A). To assess the biological relevance of HDAC5 depletion in cancer cells, a proliferation assay was performed on HCT116 human colorectal carcinoma cells. Cells were treated twice (Figure 10C) with P-G-M containing HDAC5 or control GL3 siRNA, then reseeded at equal densities and harvested at the indicated time-points. As shown in Figure 10C, the HDAC5 mRNA shutdown leads to a significant decrease of cancer cells proliferation. To assess the relative HDAC protein expression at different time points of the proliferation curve, Western blot was performed and showed a high decrease of HDAC expression. This protein shut down is the highest after 48 h and is correlated to mRNA expression values (Figure 10E).

Contrarily, one treatment with PEGylated polymers is not enough to reduce significantly the expression of HDAC5 mRNA. A second treatment increased this efficiency, especially for P-G-M-PEG<sub>2000</sub> polyplexes, with a relative expression of HDAC5 mRNA decreasing to 52% (Figure 10B). However, this decrease of HDAC5 mRNA expression of around 50% for two treatments of P-G-M-PEG<sub>2000</sub> polyplexes, related to the HDAC protein expression decrease observed by Western blot (Figure 10F), is not sufficient enough to observe a significant decrease of cell proliferation (Figure 10D).

## 4. DISCUSSION

The objective of this work was to evaluate PEGylated and functionalized aliphatic polycarbonate polyplex nanoparticles to administer intravenously HDAC5 siRNA to tumor cells, in order to decrease their proliferation. We compared newly synthesized P-G-M-PEG<sub>750</sub> and P-G-M-PEG<sub>2000</sub> polymers to non-PEGylated P-G-M polymer, for which *in vitro* efficiency has been shown previously.<sup>25</sup> 2000 Da PEG chain is described in the literature as sufficient to provide stealth properties to nanoparticles.<sup>43</sup> However, PEG is also known to limit interactions with cellular membranes and thus efficiency of polyplexes. For this reason, a shorter PEG chain of 750 Da was also used to limit this possible decrease in efficiency along with keeping sufficient stealth properties.

First, physicochemical characteristics of polyplexes were determined in order to evaluate the influence of covalently linked PEG chain to P-G-M polymer on polyplexes formation. The effect of different N/P ratios (between 10 and 60) on siRNA encapsulation rates, polyplex size and surface charge was tested. In order to be under suitable conditions for a future IV administration of the polyplexes, these effects were measured in a buffer (pH 7.4), isotonized with mannitol. Indeed, as shown by Machinskaya et al.<sup>52</sup> the physiological ionic strength may play important roles in the case of polyplexes used in gene transfection in terms of stability and destabilization of the polynucleotide component. As expected, we observed an

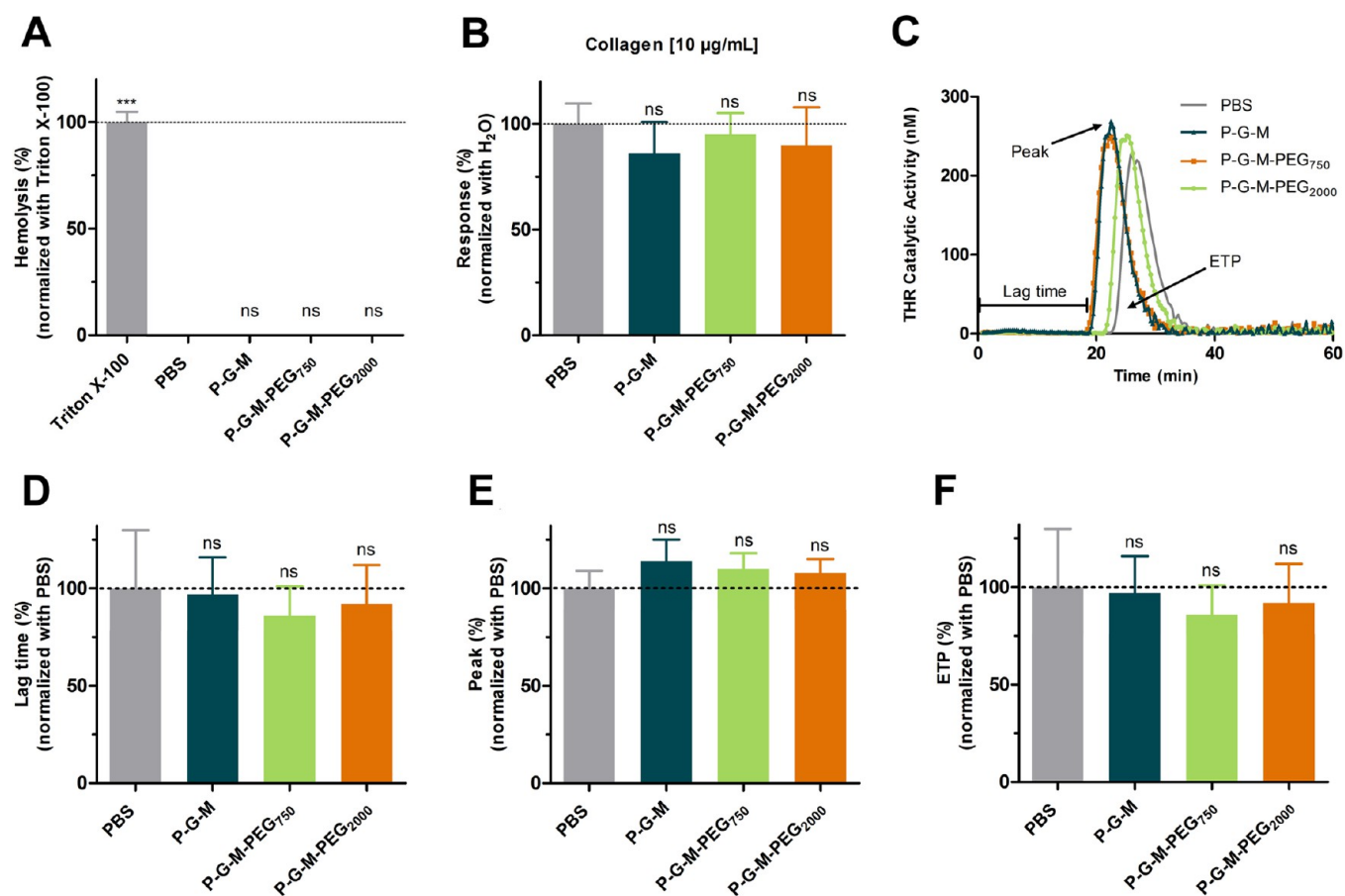


**Figure 7.** Hemocompatibility assays of polyplex nanoparticles, performed at a final concentration of siRNA of 100 nM. (A) Human RBC lysis (% of hemolysis) in whole blood after 1.5 h incubation. Triton X-100 1% and PBS were respectively used as positive and negative controls. (B) Platelet aggregation induced by collagen in the presence of the different formulations. PBS is used as negative control. Results are expressed as % of response, normalized to PBS. (C) Representative thrombin activity profile induced by tissue factor in the presence of nanoparticles or PBS (negative control). Control parameters (lag time (D), peak (E), and ETP (F)) of these thrombin activity profiles were expressed as %, normalized to PBS values. Statistical comparisons with negative controls were performed by using one-way ANOVA, followed by the Dunnett's test.

increase in the encapsulation with the increase of the N/P ratio, that the sizes of the polyplexes stabilize from a certain N/P and that the surface charge gradually increases to reach a plateau also from a certain N/P. The N/P 40 selected corresponds, for the three tested polymers, to the N/P which allows the encapsulation of almost 100% of the siRNA, to form polyplexes with a stable size compatible with IV administration and to reach the surface charge plateau. N/P 40 is the minimum ratio allowing to combine these optimal characteristics for IV administration while avoiding an excess of cationic polymer and therefore of positive charges even if some of the cationic charges may remain as free polycations.

PEGylated and non-PEGylated polycarbonate polymers are able to form polyplex nanoparticles possessing physicochemical characteristics required for IV administration (Table 2).<sup>53</sup> In terms of size, diameter is slightly lower for PEGylated nanoparticles, around 150 nm, compatible with passive targeting through the "EPR effect."<sup>18</sup> As expected,  $\zeta$ -potential decreases with the presence of PEG, according to chain length, from +11.2 mV for P-G-M nanoparticles to +5 mV for P-G-M-PEG<sub>2000</sub> polyplexes. This positive charge is helpful to interact with plasma membrane.<sup>54</sup> Unlike the PEGylated particles, P-G-M polyplexes have a tendency to form aggregates, as shown by TEM (Figure 2), because of too low electrostatic and steric repulsion between these nanoparticles. In terms of electrostatic

repulsion, a colloidal suspension is considered unstable if the  $\zeta$ -potential value is between  $-30$  and  $+30$  mV.<sup>55</sup> This lower stability has been confirmed by DLS, showing a size increase over time, especially for non-PEGylated polyplexes (Figure S2). Nuclease resistance assay shows a protection of the siRNA in the three polyplexes formulations. PEGylated and non-PEGylated polycarbonate polymers form nanoparticles with good physicochemical characteristics but the presence of PEG seems to increase colloidal stability proportionally to chain length, thanks to steric hindrance.<sup>56</sup>

As PEG was added on the P-G-M polymer structure in order to decrease interactions with blood constituents, different techniques were used to evaluate interactions between polyplexes nanoparticles and plasma proteins.

First, ITC study has been used to evaluate interaction of polyplex nanoparticles with BSA, used as blood reference protein. According to the results (Figure 4), we can conclude that the three polyplex formulations cannot be clearly distinguished regarding their binding properties with BSA. Only PEG<sub>2000</sub> statistically reduces the affinity between particles and BSA compared to non-PEGylated particles. However, all the values are low and the observed difference should not be significant *in vivo*. As shown by Leclercq et al.,<sup>42</sup> even if albumin adsorption is minimized by the presence of PEG, albumin layers are present on both pegylated and nonpegylated surfaces,

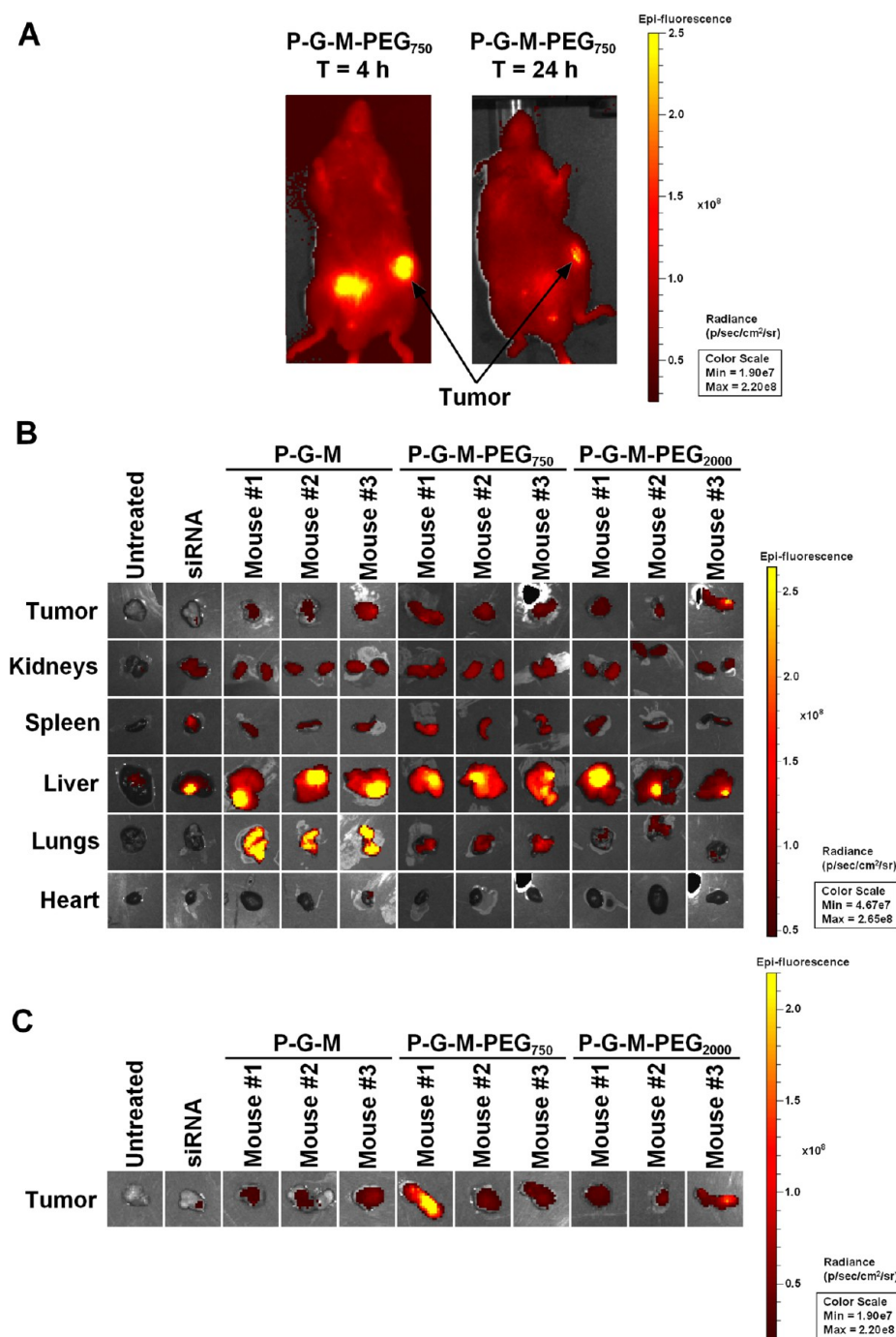


**Figure 8.** *In vivo* biodistribution of Alexa Fluor 660 labeled HDAC5 siRNA on mice. (A) Fluorescence intensity on living mice, 4 and 24 h post IV injection of 1 mg/kg fluorescent siRNA in P-G-M-PEG<sub>750</sub> nanoparticles. (B) *Ex vivo* imaging on tumors and principal organs performed 4 h post IV injection of 1 mg/kg of free siRNA, or complexed in P-G-M, P-G-M-PEG<sub>750</sub>, or P-G-M-PEG<sub>2000</sub> nanoparticles. (C) *Ex vivo* imaging on the same tumors but with a narrower fluorescence scale.

even if it is in different amounts. The repulsive effect assigned to pegylated surfaces in contact with blood is probably due to the presence of adsorbed albumin even if the deposition of this protein from blood is likely to be not as specific as when the albumin is alone in solution according to data collected for mixtures of proteins.

As explained in the introduction, the negatively charged proteins present in the FBS can compete with the siRNA complexation.<sup>37</sup> At a concentration of 10% FBS, the competition highlights the difference of affinity between polymers and siRNA (Figure 5A). The lower release of

siRNA from P-G-M polyplex nanoparticles compared to PEGylated ones can be explained by a stronger electrostatic interaction between the positively charged polymer and negatively charged siRNA. Indeed, the presence of PEG groups grafted on the polymer may hamper the formation of electrostatic interactions with the siRNA. In the presence of 50% FBS, around 50% of siRNA is released from polyplexes nanoparticles already after 1 h (Figure 5B). Similar values were observed for all polyplex nanoparticles, PEGylated or not, due to the presence of a high amount of negatively charged proteins, which strongly compete with siRNA on the binding to

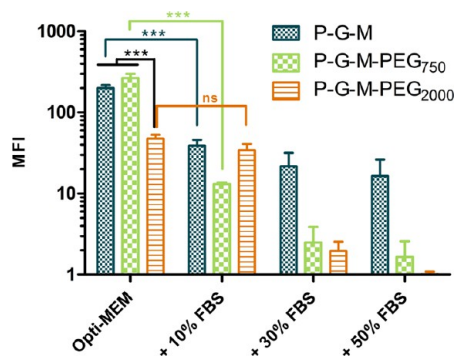


**Figure 9.** Cellular uptake in serum-free medium and in the presence of different concentrations of FBS. Mean fluorescence intensity (MFI) of HeLa cells treated with polyplexes nanoparticles containing fluorescent siRNA, after 1 h of incubation in Opti-MEM containing 0, 10, 30, or 50% FBS at 37 °C. MFI is normalized to untreated control cells. Statistical analysis was performed by using two-way ANOVA, followed by a Bonferroni's test.

the polymer.<sup>37</sup> At high FBS concentration, the competition is saturated and no difference can be seen between formulations. As the competition phenomenon is saturated, the complexation rate remains constant up to 3 h. The fact that 50% of the siRNA remains associated with the polymer after 3 h of incubation in a protein-rich environment indicates relatively stable nanovectors in terms of cargo release.<sup>37,57,58</sup> However, *in vitro* the concentration of interacting proteins is fixed. In blood, releasing proteins will be renewed and thus all the siRNA should be released. Moreover, *in vivo*, a Vroman effect may be feared meaning that some proteins with higher affinity will lead to stable combinations which will result in the release of the siRNA.

According to fSPT results (Figure 5C–E), a size increase is observed over time for the non-PEGylated nanoparticles in the presence of 10% serum, probably because of the formation of aggregates. If a major population of polyplexes remains in a size range compatible with intravenous administration (<300 nm), particles with 1  $\mu\text{m}$  are also present at 3 h.<sup>53</sup> P-G-M-PEG<sub>750</sub> and P-G-M-PEG<sub>2000</sub> nanoparticles also exhibit an initial growth due to the presence of 10% serum, higher for P-G-M-PEG<sub>2000</sub> than for P-G-M-PEG<sub>750</sub>. However, their size is stable over time and does not increase anymore after 1 h of contact with the serum components. PEG does not appear to completely prevent the formation of the protein corona around polyplexes but appears to have a role in the stability of the particle size over time.

Overall, differences in the behavior of the PEGylated of non-PEGylated formulations in the presence of serum are negligible. Surprisingly, P-G-M polyplexes show moderate interactions with plasma proteins. One possible explanation is that the morpholine block of the polycarbonate polymer is on the surface of P-G-M polyplexes. This block is hydrophilic but not charged at a neutral pH, and thus can play a role similar to PEGylation. Forming a hydrated corona around the nanoparticle, neutral morpholine block could reduce interactions between the anionic proteins and cationic guanidine functions.<sup>44</sup>

To validate the *in vitro* assays showing negligible differences between the three formulations, biodistribution study on mice after IV injection was performed to highlight *in vivo* differences between PEGylated and non-PEGylated nanoparticles. Considering that these polyplex nanoparticles cause no cytotoxicity

endothelial cells (Figure 6) and have no effect on both hemolysis and coagulation (Figure 7), their intravenous injection can be considered without alterations of normal blood function. These results have a high importance, since a release of hemoglobin can lead to adverse effects, like renal toxicity, anemia, and pulmonary hypertension.<sup>59</sup> The *in vivo* study showed an accumulation of polyplex nanoparticles at the tumor site thanks to the EPR effect, compared to naked siRNA, despite accumulation in certain organs such as the liver and spleen (Figure 8). These organs possess a fenestrated vasculature and are able to capture a certain proportion of the nanoparticles with a diameter higher than 200 nm.<sup>53</sup> As observed previously by others,<sup>40</sup> P-G-M polyplexes exhibit pulmonary accumulation due to the retention of aggregates in the small capillaries of the lungs. Indeed, it is often described that particles in the micrometer range exhibit rapid accumulation in these capillaries.<sup>53</sup> It would therefore appear that in the presence of blood, P-G-M polyplexes may form larger aggregates than those observed in the presence of 10% serum. Differences in fluorescence intensities between the three different tumors have been observed for P-G-M-PEG<sub>750</sub> (Figure 8C). Exploiting the EPR effect remains the main basis for targeted delivery of intravenously injected nanomedicines to tumors. Features of tumor blood vessels such as the extent of tumor neovascularization, degree of vessel maturation, vasculature (dis)organization, dilatations, fenestrations, and gap junctions coupled with the tumor size, the presence of necrotic and hypoxic tissues and the intensity of interstitial matrix density might influence the EPR effect and therefore the uniform biodistribution and tumor accumulation of nanoparticles.

Addition of PEG seems here to promote the passive tumor targeting and decrease lung accumulation, probably because of higher blood stability of PEGylated polyplexes. But these results show no difference between the PEG<sub>750</sub> and PEG<sub>2000</sub>. Addition of PEG is necessary in order to avoid occlusion of pulmonary capillaries and lethal toxicity.<sup>40</sup> However, these results should be interpreted with caution because of the small number of mice tested.

It is known that PEGylation can partially mask the positive surface charge of polyplexes, with a consequent reduction of the interaction of nanoparticles with the plasma proteins, but also with the cellular membranes.<sup>60,61</sup> This dilemma can result in a decrease of the efficiency by decreasing cellular uptake and endosomal escape, in proportion to the chain length and density.<sup>62</sup> The possible decrease in cellular uptake and mRNA degradation has been therefore tested *in vitro*.

Cellular uptake in serum-free conditions (Opti-MEM) is decreased for P-G-M-PEG<sub>2000</sub> compared to P-G-M and P-G-M-PEG<sub>750</sub> polyplexes. This decrease is probably due to weaker interactions with cells because of large PEG chain, masking the surface of polyplex nanoparticles.<sup>61</sup> However, PEG<sub>750</sub> does not seem to reduce interaction between polyplexes and cell membrane, probably due to the shorter chain length.<sup>43</sup>

To be closer to physiological conditions, cellular uptake has been performed in the presence of serum. Indeed, the presence of a protein-rich environment can cause a loss of activity *in vitro*, compared to serum-free conditions.<sup>63</sup> In the presence of serum, cellular uptake of the three formulations is greatly reduced, compromising the efficiency of these polyplexes in biological conditions. Clearly, P-G-M polyplexes cellular uptake is less influenced by the presence of high amounts of FBS. The decrease in cellular uptake can generally be explained by (i) a

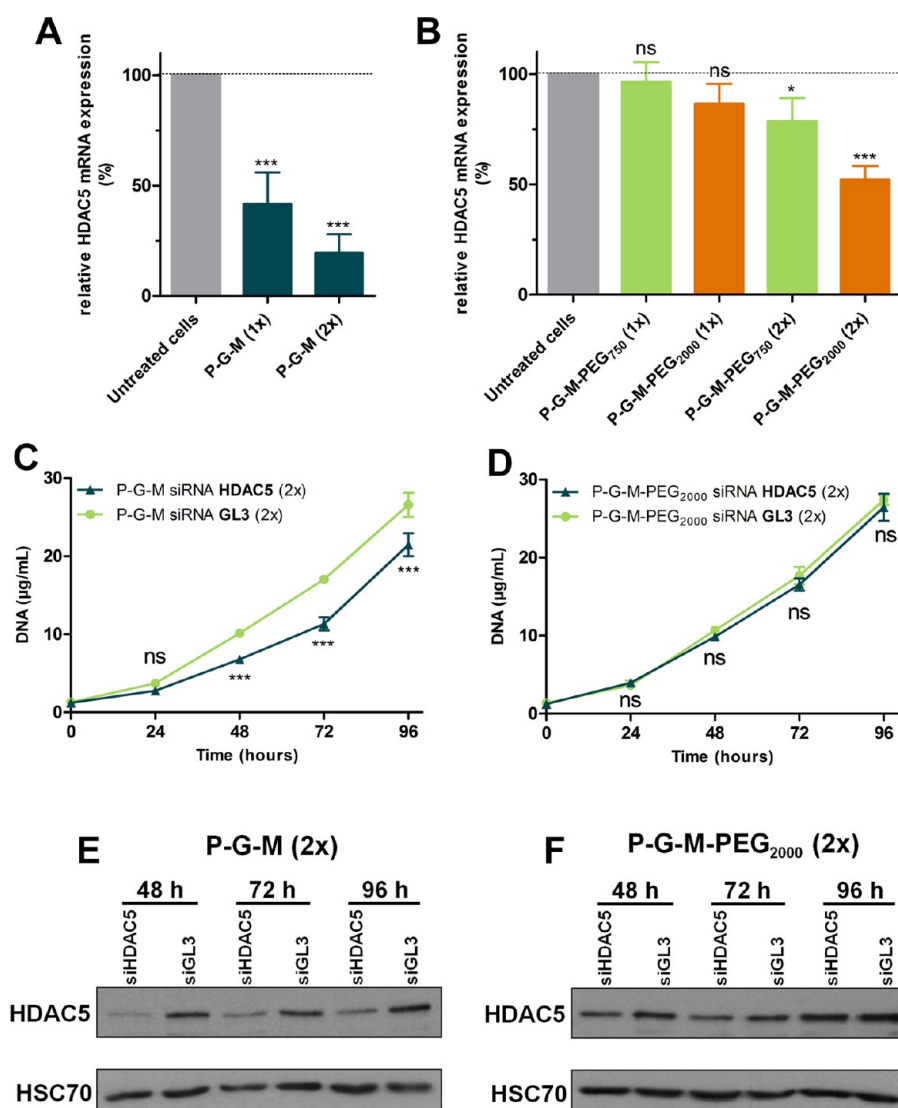


**Figure 10.** *In vitro* efficiency of polyplex nanoparticles. Relative HDAC5 mRNA expression in HeLa cells determined by RT-qPCR 48 h after the first transfection with P-G-M (A), or P-G-M-PEG<sub>750</sub> and P-G-M-PEG<sub>2000</sub> (B) polyplexes, treated 1 or 2 times. Values were normalized to  $\beta$ -actin, and expressed relative to the value of irrelevant siRNA-transfected. Statistical analysis was performed by using one-way ANOVA, followed by a Dunnett's test compared to control value of 100%. Proliferation assay on HCT116 cells after two treatments with P-G-M (C) or P-G-M-PEG<sub>2000</sub> polyplexes (D). Statistical analysis was performed by using one-way ANOVA, followed by a Bonferroni's test compared to the related GL3 control condition. Only cells treated with P-G-M polyplexes showed a significant decrease in proliferation. Silencing of HDAC5 protein in HCT116 cells treated with P-G-M (E) and P-G-M-PEG<sub>2000</sub> (F) polyplexes, at different time points of the proliferation curves.

premature release of siRNA from nanoparticles in the presence of FBS, (ii) an increase of the size that can interfere with endocytosis mechanisms, and/or (iii) the formation of a protein corona on the surface of polyplexes that can modify the surface properties of nanoparticles and their ability to interact with plasma membranes.<sup>63–65</sup> In the case of PEGylated and non-PEGylated P-G-M nanoparticles, the uptake differences cannot be explained by a different release of siRNA or increase of polyplex size, according to Figure 5. Differences in the protein-corona composition could explain differences in uptake of PEGylated and non-PEGylated nanoparticles in concentrated FBS medium.<sup>64</sup> Anyhow, these data suggest that such a reduction in cellular entry might be associated with a loss of efficiency compared to serum-free *in vitro* conditions.

*In vitro*, P-G-M polyplex nanoparticles are able to deliver siRNA into the cytoplasm to degrade HDAC5 mRNA in serum-free conditions, leading to a protein shutdown and a

decrease in proliferation of cancer cells (Figure 10A,C,E). However, PEGylated polyplex nanoparticles have a lower *in vitro* efficiency in terms of decrease of HDAC5 mRNA and protein expression, compared to non-PEGylated nanoparticles. This decrease of mRNA shutdown efficiency leads to the loss of the antiproliferative effect on cancer cells obtained for P-G-M nanoparticles (Figure 10B,D,F).

In this study, the efficiency of P-G-M-PEG<sub>2000</sub> is higher than that of P-G-M-PEG<sub>750</sub>, despite the lower cellular uptake. A possible explanation to this observation is the difference of the morpholine/guanidine ratio between these two polymers. For P-G-M-PEG<sub>2000</sub> polymer, the ratio is 1.5, compared to 1.2 for P-G-M-PEG<sub>750</sub> (Table 1). Previously, we showed that the buffer capacity of the polymer is directly related to this ratio,<sup>25</sup> resulting in a possible higher endosomal escape for P-G-M-PEG<sub>2000</sub> than for P-G-M-PEG<sub>750</sub>, counterbalancing the lowest cellular uptake. However, P-G-M and P-G-M-PEG<sub>750</sub> nano-

particles show similar cellular uptake in serum-free conditions and similar buffer capacity (Table 1). Differences of efficiency between these two polyplex nanoparticles are probably due to more complex intracellular mechanisms influenced by PEGylation that will require further investigations.<sup>62</sup>

According to *in vitro* efficiency and cellular uptake in the presence of FBS, *in vivo* efficacy of PEGylated polyplexes seems compromised. Contrariwise, non-PEGylated polyplex nanoparticles seem to keep a part of their capacity to enter into cells in serum rich conditions and have good *in vitro* efficacy. In view of these results, non-PEGylated polyplex seems therefore more promising than PEGylated polyplex for *in vivo* efficacy. However, as shown by the *in vivo* study, these polymers appear to have a lesser accumulation in the tumor and a large unexplained accumulation in the lungs. Before considering *in vivo* efficacy using this polymer, it will be necessary to understand the reasons and the risks linked to this unexplained pulmonary accumulation.

## 5. CONCLUSIONS

Although PEGylation is used in the clinic to increase the biological half-life and tumor passive targeting of clinically used liposomes-based nanoparticles, like Caelyx, Doxil, and Lip-oDox,<sup>66</sup> this strategy seems to be not suitable for siRNA delivery. This paper raises the question of the relevance of this commonly described PEGylation strategy for siRNA delivery. Indeed, compared to small molecules like doxorubicin that are able to diffuse through cellular membranes after its release from the nanoparticle at the tumor site, siRNA needs to be complexed with its vector to cross cellular membranes, escape from the endosome and reach the cytoplasm.<sup>67</sup> Unfortunately, PEGylation seems to interfere with these crucial steps for effective siRNA delivery.<sup>60,62</sup> Moreover, our work highlights the necessity of carrying out *in vitro* tests in conditions closer to the physiological conditions than those conventionally used. This will allow to understand the *in vivo* studies and the numerous disappointments that result from them. The physicochemistry plays an important role in these phenomena and the literature is questionable when it forgets to take into account the interactions with blood and endothelial elements to consider *in vitro* investigations only.

Because of this “PEG dilemma,” other strategies than classical PEGylation should perhaps also be considered in order to form nanoparticles with stealth properties and low protein interaction combined with high cellular uptake and biological efficiency in the presence of biological fluids, in order to combine tumor targeting and biological efficacy. One strategy could be the use of a labile bond between the PEG chain and the copolymer. This labile bond should be preferentially broken once the particle reaches the tumor site, exploiting tumor microenvironment, such as the decrease of the pH,<sup>68</sup> or the overexpression of an enzyme, like the metalloproteinase.<sup>69</sup> Another strategy could be the use of alternative polymers, noncovalently linked to the surface polyplexes, like hyaluronic acid, a biocompatible and nonimmunogenic natural polymer. In addition to conferring steric hindrance and a negative charge to the surface of polyplexes, causing repulsion with plasma proteins, hyaluronic acid has a role of targeting ligand through the overexpression of CD44 receptor on the surface of many cancer cells.<sup>70</sup> We are currently investigating this alternative strategy.

In the field of HDAC and cancer therapy, researchers and clinicians do postulate that isotype-specific HDAC inhibitors

will result in more effective drugs, leading to development of plenty new specific and selective pharmacological molecules by pharmaceutical company. HDAC5 is emerging as a strong candidate for selective pharmacologic target inhibition in the oncology setting but some concerns exist about the ultimate goal of designing a pharmacological compound that selectively target this HDAC. Although a lot of work remains to be done to further improve the efficacy of these nanoparticles, HDAC inhibition-based cancer therapy might benefit from such delivery system to specifically target HDAC members soon.

## ■ ASSOCIATED CONTENT

### 📄 Supporting Information

The Supporting Information is available free of charge on the ACS Publications website at DOI: 10.1021/acsami.6b15064.

Evolution of siRNA complexation, size and  $\zeta$ -potential of nanoparticles according to the N/P ratio (Figure S1), freeze-drying and long-term stability (Figure S2), size stability measured by DLS in the presence of serum (FBS) (Figure S3 and S4), and supplementary hemocompatibility results (Figure S5) (PDF)

## ■ AUTHOR INFORMATION

### Corresponding Author

\*E-mail: [geraldine.piel@ulg.ac.be](mailto:geraldine.piel@ulg.ac.be), Phone: +3243664308, Fax: +3243664302.

### ORCID

Antoine Frère: 0000-0002-2837-7470

### Author Contributions

G. Piel and D. Mottet contributed equally to this work.

### Notes

The authors declare no competing financial interest.

## ■ ACKNOWLEDGMENTS

The authors thank the Belgium National Fund for Scientific Research (<http://www.frs-fnrs.be>), TELEVIE, the Centre Anti-Cancéreux and Fonds Léon Frédéricq près de l'Université de Liège for funding. The authors thank the GIGA “animal” core facility, Fabrice Olivier, Marie Dehuy, Natacha Leroi, Jonathan Cimino and Maud Vandereyken for their help during *in vivo* experiments as well as the GIGA “Cell Imaging and Flow Cytometry” core facility for their help with flow cytometry. CIRMAP is grateful to the “Belgian Federal Government Office Policy of Science (SSTC)” for general support in the frame of the PAI-7/05, the European Commission and the Wallonia Region (FEDER Program) and OPTI2MAT program of excellence. D.M. is research associate at the National Fund for Scientific Research (FNRS). E.H. is a FNRS-TELEVIE fellow. A.F. and A.B. are FNRS fellows.

## ■ REFERENCES

- (1) Glozak, M. A.; Seto, E. Histone Deacetylases and Cancer. *Oncogene* **2007**, *26*, 5420–5432.
- (2) Zhang, L.; Han, Y.; Jiang, Q.; Wang, C.; Chen, X.; Li, X.; Xu, F.; Jiang, Y.; Wang, Q.; Xu, W. Trend of Histone Deacetylase Inhibitors in Cancer Therapy: Isoform Selectivity or Multitargeted Strategy. *Med. Res. Rev.* **2015**, *35*, 63–84.
- (3) Mottamal, M.; Zheng, S.; Huang, T. L.; Wang, G. Histone Deacetylase Inhibitors in Clinical Studies as Templates for New Anticancer Agents. *Molecules* **2015**, *20*, 3898–3941.
- (4) Zhang, J.; Zhong, Q. Histone Deacetylase Inhibitors and Cell Death. *Cell. Mol. Life Sci.* **2014**, *71*, 3885–3901.

- (5) Chun, P. Histone Deacetylase Inhibitors in Hematological Malignancies and Solid Tumors. *Arch. Pharmacol. Res.* **2015**, *38*, 933–949.
- (6) Finnin, M. S.; Donigian, J. R.; Cohen, A.; Richon, V. M.; Rifkind, R. A.; Marks, P. A.; Breslow, R.; Pavletich, N. P. Structures of a Histone Deacetylase Homologue Bound to the TSA and SAHA Inhibitors. *Nature* **1999**, *401*, 188–193.
- (7) Peixoto, P.; Castronovo, V.; Matheus, N.; Polese, C.; Peulen, O.; Gonzalez, A.; Boxus, M.; Verdin, E.; Thiry, M.; Dequiedt, F.; Mottet, D. HDAC5 Is Required for Maintenance of Pericentric Heterochromatin, and Controls Cell-Cycle Progression and Survival of Human Cancer Cells. *Cell Death Differ.* **2012**, *19*, 1239–1252.
- (8) Fan, J.; Lou, B.; Chen, W.; Zhang, J.; Lin, S.; Lv, F. F.; Chen, Y. Down-Regulation of HDAC5 Inhibits Growth of Human Hepatocellular Carcinoma by Induction of Apoptosis and Cell Cycle Arrest. *Tumor Biol.* **2014**, *35*, 11523–11532.
- (9) Liu, J.; Gu, J.; Feng, Z.; Yang, Y.; Zhu, N.; Lu, W.; Qi, F. Both HDAC5 and HDAC6 Are Required for the Proliferation and Metastasis of Melanoma Cells. *J. Transl. Med.* **2016**, *14*, 7–19.
- (10) Fire, A.; Xu, S.; Montgomery, M. K.; Kostas, S. A.; Driver, S. E.; Mello, C. C. Potent and Specific Genetic Interference by Double-Stranded RNA in *Nature* **1998**, *391*, 806–811.
- (11) Elbashir, S. M.; Harborth, J.; Lendeckel, W.; Yalcin, A.; Weber, K.; Tuschl, T. Duplexes of 21-Nucleotide RNAs Mediate RNA Interference in Cultured Mammalian Cells. *Nature* **2001**, *411*, 494–498.
- (12) Oh, Y. K.; Park, T. G. siRNA Delivery Systems for Cancer Treatment. *Adv. Drug Delivery Rev.* **2009**, *61*, 850–862.
- (13) Corbet, C.; Raggelle, H.; Pourcelle, V.; Vanvarenberg, K.; Marchand-Brynaert, J.; Pr at, V.; Feron, O. Delivery of siRNA Targeting Tumor Metabolism Using Non-Covalent Pegylated Chitosan Nanoparticles: Identification of an Optimal Combination of Ligand Structure, Linker and Grafting Method. *J. Controlled Release* **2016**, *223*, 53–63.
- (14) Daka, A.; Peer, D. RNAi-Based Nanomedicines for Targeted Personalized Therapy. *Adv. Drug Delivery Rev.* **2012**, *64*, 1508–1521.
- (15) Ambardekar, V. V.; Han, H. Y.; Varney, M. L.; Vinogradov, S. V.; Singh, R. K.; Vetro, J. A. The Modification of siRNA with 3' Cholesterol to Increase Nuclease Protection and Suppression of Native mRNA by Select siRNA Polyplexes. *Biomaterials* **2011**, *32*, 1404–1411.
- (16) Bertrand, N.; Leroux, J. C. The Journey of a Drug-Carrier in the Body: An Anatomical-Physiological Perspective. *J. Controlled Release* **2012**, *161*, 152–163.
- (17) Varkouhi, A. K.; Scholte, M.; Storm, G.; Haisma, H. J. Endosomal Escape Pathways for Delivery of Biologicals. *J. Controlled Release* **2011**, *151*, 220–228.
- (18) Fang, J.; Nakamura, H.; Maeda, H. The EPR Effect: Unique Features of Tumor Blood Vessels for Drug Delivery, Factors Involved, and Limitations and Augmentation of the Effect. *Adv. Drug Delivery Rev.* **2011**, *63*, 136–151.
- (19) Xiang, S.; Tong, H.; Shi, Q.; Fernandes, J. C.; Jin, T.; Dai, K.; Zhang, X. Uptake Mechanisms of Non-Viral Gene Delivery. *J. Controlled Release* **2012**, *158*, 371–378.
- (20) Barua, S.; Mitragotri, S. Challenges Associated with Penetration of Nanoparticles across Cell and Tissue Barriers: A Review of Current Status and Future Prospects. *Nano Today* **2014**, *9*, 223–243.
- (21) Tempelaar, S.; Mespouille, L.; Coulembier, O.; Dubois, P.; Dove, A. P. Synthesis and Post-Polymerisation Modifications of Aliphatic Poly(Carbonate)s Prepared by Ring-Opening Polymerisation. *Chem. Soc. Rev.* **2013**, *42*, 1312–1336.
- (22) Chen, W.; Meng, F.; Cheng, R.; Deng, C.; Feijen, J.; Zhong, Z. Advanced Drug and Gene Delivery Systems Based on Functional Biodegradable Polycarbonates and Copolymers. *J. Controlled Release* **2014**, *190*, 398–414.
- (23) Ong, Z. Y.; Fukushima, K.; Coody, D. J.; Yang, Y. Y.; Ee, P. L.; Hedrick, J. L. Rational Design of Biodegradable Cationic Polycarbonates for Gene Delivery. *J. Controlled Release* **2011**, *152*, 120–126.
- (24) de la Rosa, V. R.; Tempelaar, S.; Dubois, P.; Hoogenboom, R.; Mespouille, L. Poly(2-Ethyl-2-Oxazoline)-Block-Polycarbonate Block Copolymers: From Improved End-Group Control in Poly(2-Oxazoline)s to Chain Extension with Aliphatic Polycarbonate through a Fully Metal-Free Ring-Opening Polymerisation Process. *Polym. Chem.* **2016**, *7*, 1559–1568.
- (25) Fr ere, A.; Kawalec, M.; Tempelaar, S.; Peixoto, P.; Hendrick, E.; Peulen, O.; Evrard, B.; Dubois, P.; Mespouille, L.; Mottet, D.; Piel, G. Impact of the Structure of Biocompatible Aliphatic Polycarbonates on siRNA Transfection Ability. *Biomacromolecules* **2015**, *16*, 769–779.
- (26) Geihe, E. I.; Cooley, C. B.; Simon, J. R.; Kiesewetter, M. K.; Edward, J. A.; Hickerson, R. P.; Kaspar, R. L.; Hedrick, J. L.; Waymouth, R. M.; Wender, P. A. Designed Guanidinium-Rich Amphiphilic Oligocarbonate Molecular Transporters Complex, Deliver and Release siRNA in Cells. *Proc. Natl. Acad. Sci. U. S. A.* **2012**, *109*, 13171–13176.
- (27) Bartolini, C.; Mespouille, L.; Verbruggen, I.; Willem, R.; Dubois, P. Guanidine-Based Polycarbonate Hydrogels: From Metal-Free Ring-Opening Polymerization to Reversible Self-Assembling Properties. *Soft Matter* **2011**, *7*, 9628–9637.
- (28) Reschner, A.; Shim, Y. H.; Dubois, P.; Delvenne, P.; Evrard, B.; Marcelis, L.; Moucheron, C.; Kirsch-De Mesmaeker, A.; Defranco, E.; Raes, M.; Piette, J.; Collard, L.; Piel, G. Evaluation of a New Biocompatible Poly(N-(Morpholino Ethyl Methacrylate)-Based Copolymer for the Delivery of Ruthenium Oligonucleotides, Targeting HPV16 E6 Oncogene. *J. Biomed. Nanotechnol.* **2013**, *9*, 1432–1440.
- (29) Zhao, Z. X.; Gao, S. Y.; Wang, J. C.; Chen, C. J.; Zhao, E. Y.; Hou, W. J.; Feng, Q.; Gao, L. Y.; Liu, X. Y.; Zhang, L. R.; Zhang, Q. Self-Assembly Nanomicelles Based on Cationic mPEG-PLA-b-Polyarginine(R15) Triblock Copolymer for siRNA Delivery. *Biomaterials* **2012**, *33*, 6793–6807.
- (30) Omedes Pujol, M.; Coleman, D. J. L.; Allen, C. D.; Heidenreich, O.; Fulton, D. A. Determination of Key Structure–Activity Relationships in siRNA Delivery with a Mixed Micelle System. *J. Controlled Release* **2013**, *172*, 939–945.
- (31) Li, J.; Chen, Q.; Zha, Z.; Li, H.; Toh, K.; Dirisala, A.; Matsumoto, Y.; Osada, K.; Kataoka, K.; Ge, Z. Ternary Polyplex Micelles with PEG Shells and Intermediate Barrier to Complexed DNA Cores for Efficient Systemic Gene Delivery. *J. Controlled Release* **2015**, *209*, 77–87.
- (32) Fukushima, K. Poly(Trimethylene Carbonate)-Based Polymers Engineered for Biodegradable Functional Biomaterials. *Biomater. Sci.* **2016**, *4*, 9–24.
- (33) Mespouille, L.; Coulembier, O.; Kawalec, M.; Dove, A. P.; Dubois, P. Implementation of Metal-Free Ring-Opening Polymerization in the Preparation of Aliphatic Polycarbonate Materials. *Prog. Polym. Sci.* **2014**, *39*, 1144–1164.
- (34) Nachtergaele, A.; Coulembier, O.; Dubois, P.; Helvenstein, M.; Duez, P.; Blankert, B.; Mespouille, L. Organocatalysis Paradigm Revisited: Are Metal-Free Catalysts Really Harmless? *Biomacromolecules* **2015**, *16*, 507–514.
- (35) Mespouille, L.; Nederberg, F.; Hedrick, J. L.; Dubois, P. Broadening the Scope of Functional Groups Accessible in Aliphatic Polycarbonates by the Introduction of Raft Initiating Sites. *Macromolecules* **2009**, *42*, 6319–6321.
- (36) Palchetti, S.; Colapicchioni, V.; Digiaco, L.; Caracciolo, G.; Pozzi, D.; Capriotti, A. L.; La Barbera, G.; Lagana, A. The Protein Corona of Circulating Pegylated Liposomes. *Biochim. Biophys. Acta, Biomembr.* **2016**, *1858*, 189–196.
- (37) Dakwar, G. R.; Zagato, E.; Delanghe, J.; Hobel, S.; Aigner, A.; Denys, H.; Braeckmans, K.; Ceelen, W.; De Smedt, S. C.; Remaut, K. Colloidal Stability of Nano-Sized Particles in the Peritoneal Fluid: Towards Optimizing Drug Delivery Systems for Intraperitoneal Therapy. *Acta Biomater.* **2014**, *10*, 2965–2975.
- (38) Gaumet, M.; Vargas, A.; Gurny, R.; Delie, F. Nanoparticles for Drug Delivery: The Need for Precision in Reporting Particle Size Parameters. *Eur. J. Pharm. Biopharm.* **2008**, *69*, 1–9.

- (39) Maeda, H.; Wu, J.; Sawa, T.; Matsumura, Y.; Hori, K. Tumor Vascular Permeability and the EPR Effect in Macromolecular Therapeutics: A Review. *J. Controlled Release* **2000**, *65*, 271–284.
- (40) de Wolf, H. K.; Luten, J.; Snel, C. J.; Oussoren, C.; Hennink, W. E.; Storm, G. In Vivo Tumor Transfection Mediated by Polyplexes Based on Biodegradable Poly(DMAEA)-Phosphazene. *J. Controlled Release* **2005**, *109*, 275–287.
- (41) Laloy, J.; Minet, V.; Alpan, L.; Mullier, F.; Beken, S.; Toussaint, O.; Lucas, S.; Dogné, J.-M. Impact of Silver Nanoparticles on Haemolysis, Platelet Function and Coagulation. *Nanobiomedicine* **2014**, *1.110.5772/59346*
- (42) Leclercq, L.; Modena, E.; Vert, M. Adsorption of Proteins at Physiological Concentrations on Pegylated Surfaces and the Compatibilizing Role of Adsorbed Albumin with Respect to Other Proteins According to Optical Waveguide Lightmode Spectroscopy (OWLS). *J. Biomater. Sci., Polym. Ed.* **2013**, *24*, 1499–1518.
- (43) Kolate, A.; Baradia, D.; Patil, S.; Vhora, I.; Kore, G.; Misra, A. PEG - a Versatile Conjugating Ligand for Drugs and Drug Delivery Systems. *J. Controlled Release* **2014**, *192*, 67–81.
- (44) Beck-Broichsitter, M.; Nicolas, J.; Couvreur, P. Design Attributes of Long-Circulating Polymeric Drug Delivery Vehicles. *Eur. J. Pharm. Biopharm.* **2015**, *97*, 304–317.
- (45) Owens, D. E., 3rd; Peppas, N. A. Opsonization, Biodistribution, and Pharmacokinetics of Polymeric Nanoparticles. *Int. J. Pharm.* **2006**, *307*, 93–102.
- (46) Cedervall, T.; Lynch, I.; Lindman, S.; Berggard, T.; Thulin, E.; Nilsson, H.; Dawson, K. A.; Linse, S. Understanding the Nanoparticle-Protein Corona Using Methods to Quantify Exchange Rates and Affinities of Proteins for Nanoparticles. *Proc. Natl. Acad. Sci. U. S. A.* **2007**, *104*, 2050–2055.
- (47) Buyens, K.; Lucas, B.; Raemdonck, K.; Braeckmans, K.; Vercammen, J.; Hendrix, J.; Engelborghs, Y.; De Smedt, S. C.; Sanders, N. N. A Fast and Sensitive Method for Measuring the Integrity of siRNA-Carrier Complexes in Full Human Serum. *J. Controlled Release* **2008**, *126*, 67–76.
- (48) Braeckmans, K.; Buyens, K.; Bouquet, W.; Vervaeke, C.; Joye, P.; De Vos, F.; Plawinski, L.; Doevre, L.; Angles-Cano, E.; Sanders, N. N.; Demeester, J.; De Smedt, S. C. Sizing Nanomatter in Biological Fluids by Fluorescence Single Particle Tracking. *Nano Lett.* **2010**, *10*, 4435–4442.
- (49) Peulen, O.; Gonzalez, A.; Peixoto, P.; Turtoi, A.; Mottet, D.; Delvenne, P.; Castronovo, V. The Anti-Tumor Effect of HDAC Inhibition in a Human Pancreas Cancer Model Is Significantly Improved by the Simultaneous Inhibition of Cyclooxygenase 2. *PLoS One* **2013**, *8*, e75102.
- (50) Turnbull, W. B.; Daranas, A. H. On the Value of C: Can Low Affinity Systems Be Studied by Isothermal Titration Calorimetry? *J. Am. Chem. Soc.* **2003**, *125*, 14859–14866.
- (51) Velazquez Campoy, A.; Freire, E. ITC in the Post-Genomic Era...? Priceless. *Biophys. Chem.* **2005**, *115*, 115–124.
- (52) Machinskaya, A. E.; Leclercq, L.; Boustta, M.; Vert, M.; Vasilevskaya, V. V. Salt Effects on Macrophase Separations in Non-Stoichiometric Mixtures of Oppositely Charged Macromolecules: Theory and Experiment. *J. Polym. Sci., Part B: Polym. Phys.* **2016**, *54*, 1717–1730.
- (53) Blanco, E.; Shen, H.; Ferrari, M. Principles of Nanoparticle Design for Overcoming Biological Barriers to Drug Delivery. *Nat. Biotechnol.* **2015**, *33*, 941–951.
- (54) Favretto, M. E.; Wallbrecher, R.; Schmidt, S.; van de Putte, R.; Brock, R. Glycosaminoglycans in the Cellular Uptake of Drug Delivery Vectors - Bystanders or Active Players? *J. Controlled Release* **2014**, *180*, 81–90.
- (55) Tantra, R.; Schulze, P.; Quincey, P. Effect of Nanoparticle Concentration on Zeta-Potential Measurement Results and Reproducibility. *Particuology* **2010**, *8*, 279–285.
- (56) Knop, K.; Hoogenboom, R.; Fischer, D.; Schubert, U. S. Poly(Ethylene Glycol) in Drug Delivery: Pros and Cons as Well as Potential Alternatives. *Angew. Chem., Int. Ed.* **2010**, *49*, 6288–6308.
- (57) Novo, L.; Takeda, K. M.; Petteta, T.; Dakwar, G. R.; van den Dikkenberg, J. B.; Remaut, K.; Braeckmans, K.; van Nostrum, C. F.; Mastrobattista, E.; Hennink, W. E. Targeted Decationized Polyplexes for siRNA Delivery. *Mol. Pharmaceutics* **2015**, *12*, 150–161.
- (58) Oliveira, A. C.; Raemdonck, K.; Martens, T.; Rombouts, K.; Simon-Vazquez, R.; Botelho, C.; Lopes, I.; Lucio, M.; Gonzalez-Fernandez, A.; Real Oliveira, M. E.; Gomes, A. C.; Braeckmans, K. Stealth Monoolein-Based Nanocarriers for Delivery of siRNA to Cancer Cells. *Acta Biomater.* **2015**, *25*, 216–229.
- (59) Rother, R. P.; Bell, L.; Hillmen, P.; Gladwin, M. T. The Clinical Sequelae of Intravascular Hemolysis and Extracellular Plasma Hemoglobin: A Novel Mechanism of Human Disease. *Jama* **2005**, *293*, 1653–1662.
- (60) Wang, T.; Upponi, J. R.; Torchilin, V. P. Design of Multifunctional Non-Viral Gene Vectors to Overcome Physiological Barriers: Dilemmas and Strategies. *Int. J. Pharm.* **2012**, *427*, 3–20.
- (61) Mishra, S.; Webster, P.; Davis, M. E. PEGylation Significantly Affects Cellular Uptake and Intracellular Trafficking of Non-Viral Gene Delivery Particles. *Eur. J. Cell Biol.* **2004**, *83*, 97–111.
- (62) Hama, S.; Itakura, S.; Nakai, M.; Nakayama, K.; Morimoto, S.; Suzuki, S.; Kogure, K. Overcoming the Polyethylene Glycol Dilemma Via Pathological Environment-Sensitive Change of the Surface Property of Nanoparticles for Cellular Entry. *J. Controlled Release* **2015**, *206*, 67–74.
- (63) Dakwar, G. R.; Braeckmans, K.; Demeester, J.; Ceelen, W.; Smedt, S. C. D.; Remaut, K. Disregarded Effect of Biological Fluids in siRNA Delivery: Human Ascites Fluid Severely Restricts Cellular Uptake of Nanoparticles. *ACS Appl. Mater. Interfaces* **2015**, *7*, 24322–24329.
- (64) Fleischer, C. C.; Payne, C. K. Nanoparticle-Cell Interactions: Molecular Structure of the Protein Corona and Cellular Outcomes. *Acc. Chem. Res.* **2014**, *47*, 2651–2659.
- (65) Hadjidemetriou, M.; Al-Ahmady, Z.; Mazza, M.; Collins, R. F.; Dawson, K.; Kostarelos, K. In Vivo Biomolecule Corona around Blood-Circulating, Clinically Used and Antibody-Targeted Lipid Bilayer Nanoscale Vesicles. *ACS Nano* **2015**, *9*, 8142–8156.
- (66) Weissig, V.; Pettinger, T. K.; Murdock, N. Nanopharmaceuticals (Part 1): Products on the Market. *Int. J. Nanomed.* **2014**, *9*, 4357–4373.
- (67) Young, S. W.; Stenzel, M.; Jia-Lin, Y. Nanoparticle- siRNA: A Potential Cancer Therapy? *Crit. Rev. Oncol. Hematol.* **2016**, *98*, 159–169.
- (68) Mo, R.; Gu, Z. Tumor Microenvironment and Intracellular Signal-Activated Nanomaterials for Anticancer Drug Delivery. *Mater. Today* **2016**, *19* (5), 274–283.
- (69) Hatakeyama, H.; Akita, H.; Kogure, K.; Oishi, M.; Nagasaki, Y.; Kihira, Y.; Ueno, M.; Kobayashi, H.; Kikuchi, H.; Harashima, H. Development of a Novel Systemic Gene Delivery System for Cancer Therapy with a Tumor-Specific Cleavable PEG-Lipid. *Gene Ther.* **2007**, *14*, 68–77.
- (70) Dufay Wojcicki, A.; Hillaireau, H.; Nascimento, T. L.; Arpicco, S.; Taverna, M.; Ribes, S.; Bourge, M.; Nicolas, V.; Bochot, A.; Vauthier, C.; Tsapis, N.; Fattal, E. Hyaluronic Acid-Bearing Lipoplexes: Physico-Chemical Characterization and in Vitro Targeting of the CD44 Receptor. *J. Controlled Release* **2012**, *162*, 545–552.